Molecular insights into the mechanism of calmodulin inhibition of the EAG1 potassium channel

Maria João Marques-Carvalho[1,2], Johannes Oppermann[3], Eva Muñoz[4], Andreia S. Fernandes[1,2], Guillaume Gabant[5], Martine Cadene[5], Stefan H. Heinemann[3], Roland Schönherr[3], João H. Morais-Cabral[1,2]

[1]IBMC, Instituto de Biologia Molecular e Celular, [2]Instituto de Investigação e Inovação em Saúde, Universidade do Porto, [3]Center for Molecular Biomedicine, Department of Biophysics, Friedrich Schiller University Jena and Jena University Hospital, [4]Software 4 Science Developments, [5]Centre de Biophysique Moléculaire, CNRS UPR430

Originally published in *Structure*. 2016 Oct 4;24(10):1742-1754. doi: 10.1016/j.str.2016.07.020.

Abstract

The human EAG1 potassium channel belongs to the superfamily of KCNH voltage-gated potassium channels that have roles in cardiac repolarization and neuronal excitability. EAG1 is strongly inhibited by Ca2+-calmodulin (CaM) through a mechanism that is not understood. We determined the binding properties of CaM with each one of three previously identified binding sites (BDN, BDC1 and BDC2), analyzed binding to protein stretches that include more than one site, and determined the effect of neighboring globular domains on the binding properties. The determination of the crystal structure of CaM bound to BDC2 shows the channel fragment interacting with only the C-lobe of calmodulin and adopting an unusual bent conformation. Based on this structure and on a functional and biochemical analysis of mutants, we propose a model for the mechanism of inhibition where the local conformational change induced by CaM binding at BDC2 is at the basis of channel modulation.

Introduction

Voltage-gated potassium channels of the KCNH family (EAG, ERG and ELK) are involved in important physiological processes like cardiac repolarization, neuronal excitability and cellular proliferation (Crociani et al., 2003; Pardo and Stuhmer, 2014; Sanguinetti and Tristani-Firouzi, 2006). These are tetrameric channels that contain large cytoplasmic regions which serve as interfaces for modulatory inputs such as phosphorylation, interaction with kinases, integrins and calmodulin (Cherubini et al., 2005; Morais-Cabral and Robertson, 2015; Schonherr et al., 2000; Sun et al., 2004; Wang et al., 2002; Warmke and Ganetzky, 1994). The cytoplasmic regions include a PAS domain on the N terminus and a domain with homology to cyclic nucleotide binding domains (CNB-homology domain, CNBhD) on the C terminus; it has been shown that the PAS domain and the CNB-homology domain interact with each other (Gustina and Trudeau, 2011; Haitin et al., 2013).

K^+ currents mediated by EAG1 channels are potently suppressed by intracellular Ca^{2+} with an IC_{50} of about 100 nM, an effect that is mediated by calmodulin with an IC_{50} of 6 nM for the Ca^{2+}-calmodulin

complex (Sahoo et al., 2010; Schonherr et al., 2000). Ca^{2+}-CaM is here referred to as CaM to contrast with Ca^{2+}-free apo-CaM. It has been proposed that binding of a single CaM complex is sufficient for inhibition of the tetrameric channel (Schonherr et al., 2000). Using a peptide array screen that spanned the whole EAG1 cytoplasmic regions, three CaM binding sequences were identified (Figure S1a): BDN, immediately after the PAS domain, and BDC1 and BDC2, just after the CNB-homology domain (Ziechner et al., 2006). Mutations that affect CaM binding to these sites result in channels that are nearly insensitive to CaM, supporting the functional importance of all sites in CaM-mediated inhibition. In addition, an in-cell FRET study showed that channels with disrupting mutations on BDN or BDC2 are still able to interact with CaM, whereas channels with mutated BDN, BDC2 and intact BDC1 no longer bind CaM (Goncalves and Stuhmer, 2010). It was also shown that the mutant CaM-EF12, i.e. a CaM in which the N-lobe EF hands 1 and 2 no not bind Ca^{2+}, is able to inhibit the hEAG1 channel, albeit with reduced potency, while the C-lobe mutant CaM-EF34 (no Ca^{2+} binding at the C-lobe) does not inhibit the channel even at a concentration of 1 µM (Ziechner et al., 2006).

Using isothermal calorimetry, we expand on the results of a previous study (Ziechner et al., 2006) and dissect the binding properties of CaM to the different sites in the EAG1 channel and to a large channel fragment that includes the CNBh domain, the BDC1 and BDC2 sites. Together with the X-ray crystal structure of the CaM-BDC2 complex and a functional and biochemical analysis of mutations in BDC2 we provide new insights into the mechanism of CaM inhibition.

Results

Interaction of calmodulin with the BDC2 site

The structural and biochemical properties of the PAS and CNBh domains from the mouse EAG1 channel are well characterized (Adaixo et al., 2013; Fernandes et al., 2016; Haitin et al., 2013; Marques-Carvalho et al., 2012). As a consequence, we decided to perform the *in-vitro* characterization of the CaM binding properties to EAG1 using the mouse channel. For the functional analysis, however, we focused on the human EAG1 channel, where Cam inhibition has been well described (Marques-Carvalho et al., 2012; Sahoo et al., 2010; Schonherr et al., 2000; Ziechner et al., 2006). Importantly, mouse and human EAG1 channels are very closely related; in the N-terminal region, which spans the PAS domain and BDN site, the two sequences differ only in 2 residues among 174, while in the C-terminal region, spanning the CNBh domain, BDC1 and BDC2 sites, sequences are 100% identical (Figure S1b and S1c).

To characterize the interaction between calmodulin and the BDC2 site, we generated two maltose-binding protein (MBP) fusions: BDC2S (S for short) where the channel fragment spans residues 733-757, and BDC2L (L for long) where it spans residues 727-764 (Figure S1c). Both channel fragments are centered on the sequence originally defined by Schönherr *et al.* (Schonherr et al., 2000). Isothermal titration calorimetry (ITC) experiments with CaM, in the presence of saturating Ca^{2+}, revealed higher affinity for BDC2L (K_D ~70 nM) relative to the BDC2S (K_D ~440 nM (Figure 1a, 1b, Table 1). The affinity increase is due to a more favorable enthalpy contribution (~-14 kcal /mol for BDC2L and ~-8 kcal/mol for BDC2S) suggesting that extra interactions are formed in the long fragment. We also noticed that removal of the MBP-tag from the BDC2S fusion by proteolytic cleavage was very inefficient in the presence of CaM, suggesting that bound CaM affects the action of the protease. As shown below, this probably results from an N-terminal shift of the CaM binding site

INSTITUTO
DE INVESTIGAÇÃO
E INOVAÇÃO
EM SAÚDE
UNIVERSIDADE
DO PORTO

Rua Alfredo Allen, 208
4200-135 Porto
Portugal
+351 220 408 800
info@i3s.up.pt
www.i3s.up.pt

relative to the originally defined sequence. As a consequence of the difficulty with protease cleavage and of the lower affinity of BDC2S we focused our studies on BDC2L.

We next assessed the contribution of individual CaM lobes to the interaction with BDC2. ITC experiments showed that the C-lobe of CaM binds almost as well as the full-length protein (K_D ~ 110 nM) and 20-fold more tightly than the N-lobe (K_D ~2.2 μM) (Figure 1c, 1d, Table 1). A mutant CaM, which is not able to bind Ca^{2+} in the N-lobe (CaM-EF12), also showed tight binding (K_D ~125 nM) (Figure S2a, Table 1), corroborating results obtained with the isolated C-lobe and demonstrating the importance of this lobe for CaM binding to BDC2. Titration experiments performed in the presence of EDTA (at 2 different temperatures: 15 ºC and 25 ºC), which ensured that calmodulin is in the Ca^{2+}-free apo state, showed very weak binding (K_D >30 μM), and hence demonstrated that CaM binding to BDC2 is Ca^{2+} dependent (Figure S2b).

Structure of Ca^{2+}-calmodulin-BDC2

The structure of BDC2L (after removing MBP) in complex with Ca^{2+}-saturated calmodulin was determined at 2.85 Å resolution (Table 2). The molecular replacement procedure involved screening a collection of coordinates for the N- and C-lobes of CaM and the best search models were the coordinates of a Ca^{2+}-bound C-lobe (from PDB 3OXQ) together with an apo-CaM N-lobe (from PDB 1CFD). The new structure shows the CaM molecule in an extended conformation, with the two lobes connected through a long helix and the BDC2 fragment sitting on the C-lobe (Figure 2a), confirming our ITC results. Despite the high concentrations of Ca^{2+} kept throughout complex formation and crystal growth, the N-lobe is in the apo form. The lack of bound Ca^{2+} is probably due to the lower ion affinity of the N-lobe (Yamniuk and Vogel, 2004) and the low pH of the crystallization condition (pH 5), which may have resulted in protonation of chemical groups involved in ion coordination. In contrast, the C-lobe adopts a bound-conformation with two calcium ions bound to the EF hands 3 and 4. Probably as a consequence of the absence of bound Ca^{2+}, some regions of the N-lobe EF-hands are ill-defined in the electron-density map and were not modeled. Using the PDBeFold server (Krissinel and Henrick, 2004) we found that the calmodulin structure that more closely resembles our structure is that of a trapped intermediate (PDB 1Y6W) in which both lobes contain Ca^{2+} but the N-lobe is locked in a apo-like conformation due to the introduction of a disulfide bridge (Grabarek, 2005).

The channel fragment that could be structurally resolved comprises residues 727 to 743 (Figure 2b, S3); no density was observed for the C-terminal end of the BDC2L (residues 744 to 764), demonstrating that the interaction site for CaM is N-terminally shifted relative to the originally described BDC2 sequence. The BDC2 channel fragment adopts an intriguing conformation in the crystal structure (Figure 2b): the first 7 residues (727-732) are in an extended conformation and run along the side of the C-lobe between two crystallographically related molecules (Figure 2c), they are followed by an ~8-residue long helix that sits on the hydrophobic cleft of the C-lobe and is positioned at ~90º relative to the N-terminal residues. The interface formed by CaM and BDC2 amounts to 531 $Å^2$; some of the BDC2 residues involved in contacts with CaM (≤ 4Å from CaM) are: P728, L729 and L731 in the N-terminal stretch, and P736, V737, R739, L740 and F741 C-terminal helix (Figure 2b). The N-terminal residues A727, L729, I730 and L731 contact a neighboring CaM molecule (Figures 2b, 2c).

There are two features in this structure that are worthwhile presenting in some detail because they appear to stabilize the complex and the BDC2 conformation. First, at the center of the CaM-BDC2

INSTITUTO
DE INVESTIGAÇÃO
E INOVAÇÃO
EM SAÚDE
UNIVERSIDADE
DO PORTO

Rua Alfredo Allen, 208
4200-135 Porto
Portugal
+351 220 408 800
info@i3s.up.pt
www.i3s.up.pt

interface there is group of apolar residues forming a "hydrophobic cluster" (Figure 2d) that includes A88, L112, M144 and M145 from CaM, V737, L740 and F741 from the C-terminal BDC2 helix), as well as L731 from the N-terminal BDC2 stretch. Second, the bending point or elbow of BDC2 (residues 732-736) includes 3 prolines and adopts a compact structure which favors van der Waals interactions and hydrogen bonding between several residues (Figure 2e); for example, the main-chain carbonyl of P736 is within hydrogen bonding distance (≤ 3.5 Å) of main-chain amino groups of R738 and R739, the same for P732 and H735 and for the side-chain of H735 and the main-chain amino group of V737.

Biochemical and functional analysis of the Ca^{2+}-calmodulin-BDC2 structure

To better define the contribution of BDC2 residues for the stability of the CaM-BDC2 complex we analyzed the impact of mutations by ITC. Double alanine mutation of V737 and L740, two residues in the hydrophobic cluster (Figure 2d), has no impact on binding affinity (K_D ~70 nM) (Figure S4a and 3ar, Table 1)). However, a double serine mutation changed affinity by 230-fold (K_D ~16 µM) (Figure S4b and 3a). Serine mutation at the neighboring F741, another residue in the cluster, changed affinity by ~28-fold (K_D ~2 µM) (Figure S4c and 3a, Table 1).

The only residue in the N-terminal extended region that participates in the hydrophobic cluster is L731 (Figure 2d); we mutated this residue together with L729, which is also in the N-terminus and interacts with CaM. Double mutation to alanine causes a ~5 kcal/mol change in binding enthalpy but had a only mild effect on affinity (K_D ~ 300 nM) (Table 1, Figure S4d and 3a). Double serine mutations at the same positions had a stronger impact, causing a ~6 kcal/mol change in binding enthalpy and reducing affinity by 10-fold (K_D ~700 nM) (Figure S4e and 3a, Table 1). Combination of L729A/L731A with R739A, a residue in the C-terminal helix of BDC2 that contacts CaM, resulted in an affinity change of 31-fold (K_D ~2µM) (Figure S4f and 3a, Table 1). Overall, these results show that residues in the N-terminal extended stretch of BDC2 contribute for the stability of the complex but the interaction is dominated by residues on the C-terminal helix.

We also assessed the functional impact of BDC2 mutations on CaM inhibition by mutating the full-length human EAG1 (hEAG1) channel and recording ion currents from wild-type and mutant channels heterologously expressed in *Xenopus* oocytes, before and after exposure to ionomycin (Figure S5). Exposure to ionomycin raises the cytoplasmic Ca^{2+} levels in two distinct phases, a fast rising Ca^{2+} concentration peak that is thought to result from a release from intracellular stores followed by a longer-sustained lower Ca^{2+} concentration level when the cation is imported from the extracellular solution (Morgan and Jacob, 1994; Yao and Tsien, 1997; Yoshida and Plant, 1992). Unlike the peak, the Ca^{2+} concentration in the plateau region is dependent on the concentration of ionomycin. The hEAG1 response to ionomycin exposure was followed by repetitive depolarizing pulses to 40 mV and the normalized steady-state current level was plotted as a function of time (Figure 3b). For the wild-type channel the plot shows a peak in current inhibition by ~70% relative to values prior exposure to ionomycin, followed by a steady-state inhibition level of ~35% in the 400-600 s time interval of ionomycin exposure. These two phases of inhibition appear to roughly follow the described evolution of cytoplasmic Ca^{2+} levels and, hence, we used the drop in channel current during the steady-state inhibition phase as an indicator of the functional Ca^{2+}-related impact on BDC2 channel mutants (Figure 3c). A report published while this work was under revision (Lorinczi et al., 2016) interprets the time-dependent reduction in inhibition not as a response to a decrease in intracellular Ca^{2+} levels but as a recovery in channel activity; however, that work uses a different

INSTITUTO
DE INVESTIGAÇÃO
E INOVAÇÃO
EM SAÚDE
UNIVERSIDADE
DO PORTO

Rua Alfredo Allen, 208
4200-135 Porto
Portugal
+351 220 408 800
info@i3s.up.pt
www.i3s.up.pt

experimental setup where oocytes are exposed to ionomycin and thapsigargin (an inhibitor of Ca^{2+}-ATPase).

Serine mutations at V710 and L713 of hEAG1 (equivalent to V737 and L740 on the BDC2 helix – Figure 2b) had a strong effect on channel inhibition, with negligible current reduction during ionomycin exposure (Figures 3b and 3c).This drastic effect reflects the large impact of the equivalent mutations (V737S/L740S) in the *in vitro* stability of the CaM-BDC2 complex (compare green bars in Figures 3a and 3c – to facilitate comparison of equivalent mutants in the mouse and human EAG1 channels data is shown with same-color bars in figures 3a and 3c). Also reflecting the biochemical results, alanine mutations at the same residues (dark-blue bars) had little effect on steady-state inhibition (~30% current decrease).

Strikingly, although mutations L729A/L731A in the N-terminal extended stretch of BDC2 had a small effect on *in vitro* complex stability (Figure 3a, red bar), the equivalent mutation in hEAG1 (L702A/L704A) caused a clear reduction of the channel's Ca^{2+} sensitivity, less than 10% current decrease during steady-state inhibition (Figures 3b and 3c, red bar). Similarly, the double alanine mutant at D734 and H735, two residues in the elbow of BDC2 (Figure 2e), had no impact on the stability of CaM-BDC2 (K_D~100 nM) (Table 1, Figure S4g and 3a, cyan bar) but a large functional impact on the hEAG1 channel (D707A/H708A), with steady-state inhibition of ~5% only (Figures 3b and 3c, cyan bar). P736A/V737A also had a very small impact on complex stability (K_D ~120 nM) (Table 1, Figure S4h and 3a, magenta), but its equivalent in hEAG1 (P709A/V710A) had a clear functional effect (steady-state inhibition ~20%) (Figure 3b and 3c, magenta). Interestingly, although the analyzed mutants in the N-terminal stretch and elbow of BDC2 have little or no impact on binding affinity, they cause in a change in binding enthalpy of ~5 kcal/mol and higher (Table 1). Current-voltage curves for mutant and wild-type hEAG1 channels showed that tested mutations did not greatly affect the voltage-dependent activation properties of the channels (Figure S5c).

Overall, the functional analysis showed that mutants with an impact on channel inhibition occur at residues spread across the BDC2 sequence: in the C-terminal helix, the N-terminal extended stretch, and in the elbow created by the bending of BDC2. This is very different from the distribution of mutants with an impact in the *in-vitro* stability of the CaM-BDC2 complex, which is focused in the C-terminal helix.

Calmodulin interaction with the BDN and BDC1 sites

To analyze the interaction between CaM and BDN we generated two MBP fusions, BDNS (residues 145-168) and BDNL (residues 138-174) (Figure S1b). ITC experiments with Ca^{2+}-saturated CaM showed that the affinity for BDNS is 10-fold lower (K_D ~180 nM) than for BDNL (K_D ~18 nM) (Figure 4a and 4b, Table 3). Unlike for BDC2, titrations with the isolated CaM lobes showed lower affinity for both lobes (N-lobe: K_D ~4.5 μM, C-lobe: K_D ~1.4 μM) (Figure 4c and 4d, Table 3), indicating that CaM interaction with BDN involves both lobes.

Cell-based FRET experiments have suggested that CaM binds to the EAG1 channel in the absence of Ca^{2+} and that this interaction occurs through BDN (Goncalves and Stuhmer, 2010). Titrations in the presence of EDTA at 15 and 25 ºC showed no detectable binding of apo-CaM to BDNL (Figure S6a). In addition, mutant CaM-EF12 binds to BDN with low affinity (K_D ~1.4 μM, Figure S6b). Overall

INSTITUTO
DE INVESTIGAÇÃO
E INOVAÇÃO
EM SAÚDE
UNIVERSIDADE
DO PORTO

Rua Alfredo Allen, 208
4200-135 Porto
Portugal
+351 220 408 800
info@i3s.up.pt
www.i3s.up.pt

this shows that the tight interaction with BDN is Ca^2-dependent and that any potential apo-CaM interaction with the EAG1 channel occurs at a yet undiscovered site.

Due to the close proximity between BDN and the PAS domain (Figure S1b) we wondered if this domain influences the interaction between CaM and BDN. We used two constructs that span the globular region of the PAS domain and the BDN binding site (Figure S1b); one construct includes most of the PAS-Cap region, a stretch of N-terminal amino acids that have a role in channel function (Cap-PAS-BDN: residues 3 to 174), while the other does not (PAS-BDN: residues 28 to 174). We found that CaM binds to both constructs with a K_D of ~100 nM (Figure S6c, S6d and Table 3), demonstrating that the PAS domain has only a slight effect on the interaction of CaM with BDN and that the PAS-Cap domains does not play a significant role in this interaction.

To analyze the interaction between CaM and BDC1 we generated a channel fragment (CNBhD-BDC1) that spans residues 552 to 724 and includes the CNBh domain plus the immediately adjacent BDC1 site (Figure S1c). Previously, using a fluorescence binding assay, we showed that CaM interacts weakly with BDC1 (Marques-Carvalho et al., 2012). We repeated this analysis with ITC and obtained a K_D ~7 μM, confirming the previous finding (Figure S7). In addition, the binding reaction is endothermic and therefore entropically driven, showing that the interaction of CaM with BDC1 is very different from the interactions with BDN or BDC2.

This conclusion led us to analyze in more detail the molecular neighborhood of BDC1. The crystal structure of the cytoplasmic assembly formed by the PAS domain and the CNBh domain shows that the BDC1 site residues are involved in the interaction between the two domains (Figure 5a). We wondered if the mutations in BDC1 that affect the CaM affinity and abolish CaM-mediated channel inhibition could also alter the stability of the PAS-CNBh domain complex. We tested this idea using a fluorescence anisotropy assay established to measure the stability of the PAS-CNBh domain complex *in vitro* (Haitin et al., 2013). Titration with wild-type CNBh domain resulted in an increase in fluorescence anisotropy of fluorescein-labeled PAS domain, which is well fitted by a binding isotherm with a K_D of 17.5 ± 6.4 μM (Figure 5b). In contrast, titration with CNBh domains that include BDC1 mutations abolishing CaM inhibition in the channel and/or reducing BDC1 affinity (R702N/R704N /R708N/K709N and I705A/V706A/F707A) had no effect on fluorescence anisotropy of PAS, showing that *in vitro* the PAS-CNBh domain complex is severely destabilized. This result therefore gives rise to an alternative explanation for the effect of the BDC1 mutations on CaM inhibition: mutations in BDC1 probably destabilize the PAS-CNBh domain complex in the channel, altering the underlying mechanism of inhibition. This suggests that the integrity of the PAS-CNBh interaction is important for the mechanism of CaM-mediated EAG1 channel inhibition and supports a recent electrophysiological analysis of hEAG1 inhibition by CaM (Lorinczi et al., 2016).

CaM interaction with a large C-terminal channel fragment

The proximity between BDC1 and BDC2, the observation that CaM binds to BDC2 through the C-lobe, and the previous suggestion that it binds to BDC1 through the N-lobe (Marques-Carvalho et al., 2012) raised the possibility that one CaM molecule can bridge the two sites. With this in mind we analyzed the interaction of CaM with a channel fragment that spans the CNBh domain, BDC1 and BDC2 (CNBhD-BDC1-BDC2, residues 552 to 764 -Figure S1c). Titration with CaM showed an isotherm with two steps and different slopes (Figure 6a). This isotherm was not satisfactorily fitted using a model with a single site (or with a set of equal sites), ruling out the idea that CaM bridges

INSTITUTO
DE INVESTIGAÇÃO
E INOVAÇÃO
EM SAÚDE
UNIVERSIDADE
DO PORTO

Rua Alfredo Allen, 208
4200-135 Porto
Portugal
+351 220 408 800
info@i3s.up.pt
www.i3s.up.pt

BDC2 and BDC1. Instead, we considered that CaM binding occurs separately at BDC1 and BDC2. Fitting the data with a model that includes two different and independent binding sites for CaM provided a satisfactory fit with potential interactions displaying K_D values of 47 nM and 5 nM (Figure 6a). However, the N values of both interactions (an indication of the interaction stoichiometry) were ~0.4, which is unexpected for a complex formed by two CaM molecules binding at different sites.

To dissect the interaction we first analyzed the binding of isolated CaM lobes and of mutant CaM-EF12 to CNBhD-BDC1-BDC2 (Figures 6b, 6c and 6d). These titrations appeared to display a single transition with a stoichiometry close to 1 and a K_D of 1.3 μM for the N-lobe, 75 nM for the C-lobe and 39 nM for CaM-EF12 (Table 3), indicating that the two-step isotherm depends on having a full-length CaM, where both lobes contain Ca^{2+} and are involved in binding. Second, we generated channel fragments that either introduce BDC1 mutations previously shown to decrease CaM affinity (R702N/R704N /R708N/K709N) (Ziechner et al., 2006) or sequentially remove the CNBh domain (BDC1-BDC2, residues 696-764) and the BDC1 site (BDC1/BDC2 linker-BDC2, residues 712-764) (Figure S1c). Isotherms of CaM titrations into these fragments clearly show the presence of two steps, demonstrating that neither the CNBh domain nor the BDC1 site is involved with this property (Figure 6e, 6f and 6g).

As a consequence of this analysis we considered a sequential binding model where CNBhD-BDC1-BDC2 binds to two different sites in CaM (the N- and C-lobes). This model (implemented in the AFFINImeter server) includes the parameter (rM) that accounts for deviations in the concentration of CNBhD-BDC1-BDC2. The final value for rM was nearly 1, indicating that the nominal concentration and stoichiometry of CNBhD-BDC1-BDC2 were correct. This supports the idea that CNBhD-BDC1-BDC2 has a single region for interaction with CaM. If it had two different sites, for example, one for the C-lobe and another for the N-lobe, we would have obtained a value close to 2 for rM (indicating two binding sites).

We refined this model further and imposed that the N- and C-lobes interact independently with the same or overlapping channel regions (Figure 7a), allowing us to extract site-specific parameters (K_D ~1.3 μM, ΔH ~ -4 kcal/mol and K_D ~7 nM, ΔH ~ -14 kcal/mol) (Figure 7b and Table 3). A species distribution plot showed that at the beginning of the titration a fraction of the CaM molecules interact through the N-lobe while others interact through the C-lobe. As CNBhD-BDC1-BDC2 is depleted, the high-affinity C-lobe out-competes the N-lobe and by the end all CaM molecules are bound through the C-lobe.

We also performed a competition experiment where C-lobe was titrated into CNBhD-BDC1-BDC2 premixed with a saturating concentration of N-lobe (Figure 7c). This titration shows a single transition, which was fitted with the single-site model implemented in Origin, resulting in a K_D ~300 nM and ΔH ~-6 kcal/mol. The affinity drop and the change in enthalpy relative to the titration of C-lobe in the absence of N-lobe show that both lobes compete for the same site in CNBhD-BDC1-BDC2. Using a competitive model implemented in AFFINImeter, which takes into consideration the enthalpy and K_D values determined previously for the N-lobe, we obtained K_D ~11 nM and ΔH ~-14 kcal/mol for the C-lobe (Figure 7c and Table 3). These values are similar to the ones obtained above for the high-affinity interaction in the two-site receptor model, supporting the model of a single site in CNBhD-BDC1-BDC2 with which the N- and C-lobes interact independently.

In addition, we performed an analysis of the CaM-(CNBhD-BDC1-BDC2) complex by native mass spectrometry (Figure S8). This revealed the presence of several forms of the complex in solution, including a 1:1 and 2:1 (CaM:channel fragment) complexes. Considering the measured affinities, the 1:1 form most likely corresponds to a complex where one CaM molecule is bound to a channel fragment at BDC2.The 2:1 complex probably corresponds to two CaM molecules bound to a channel fragment, one at BDC2 and another at BDC1. Binding of CaM to BDC1 was not apparent in our ITC analysis titration of CNBhD-BDC1-BDC2. This distinction is easily resolved if one considers the differences in the enthalpies of binding for CaM to BDC1 and BDC2. CaM binding to BDC1 has a low heat of enthalpy (ΔH ~2 kcal/mol) relative to full-length CaM, or C-lobe CaM (-14 and -10 kcal/mol, respectively; Table 1). This difference associated with a lower affinity (Table 1) most likely makes the heat contribution of the CaM-BDC1 interaction undetectable during the ITC titration of CNBhD-BDC1-BDC2.

A 2:2 form was also identified in the spectrum; it differs from the 1:1 form through the mass of its odd-charged species and in our spectrum is identified through the presence of a single peak that is not explained by other combinations of molecular masses (Figure S8). As shown above for BDC2 and proposed previously for BDC1 (Marques-Carvalho et al., 2012), binding of CaM to these sites occurs preferentially through a single lobe (N-lobe for BDC1 and C-lobe for BDC2), leaving therefore free-lobes to interact with sites in another CNBhD-BDC1-BDC2 molecule so that two CaM molecules can bridge two channel fragments, possibly in a head-to-tail arrangement.

Discussion

In this study we have dissected the binding properties of the three CaM binding sites in the EAG1 channel (BDC1, BDN and BDC2). In particular, we confirmed that the affinity of CaM for BDC1 is much lower (in the micromolar range) than for the other two sites (in the low nanomolar range). This weak interaction does not rule out a role of BDC1 in the mechanism of channel inhibition by CaM. However, we have found that mutations that affected CaM inhibition and that supported the functional importance of BDC1 also cause a destabilization of the complex between the PAS and CNBh domains. It is therefore possible that the previously described impact of these mutations on CaM inhibition does not reflect changes in the interaction of CaM with BDC1 but instead is the result of structural changes in the channel and consequent alteration of the machinery of CaM inhibition. The implication of this result is that a role of BDC1 in the mechanism of EAG1 inhibition has not been established.

Our results also show that the low nanomolar affinity (K_D ~18 nM) between CaM and BDN is dependent on the presence of the two CaM lobes, indicating that *in vitro* CaM probably adopts a canonical conformation with both lobes wrapped around the target region. In addition, although the PAS domain is positioned very close to BDN, the globular domain does not greatly affect the affinity of CaM towards BDN.

Our analysis of CaM binding to a large channel fragment (CNBhD-BDC1-BDC2) revealed that the CaM interaction with BDC2 is complex and involves competing interactions between the N- and C-lobe. Crucially we showed that the interaction between the C-lobe and BDC2 is very tight (K_D ~7 nM). The crystal structure of the CaM–BDC2 complex confirms this finding and shows an unusual conformation of the channel fragment, with the C-terminal helix of BDC2 lying in the C-lobe hydrophobic cleft of CaM and the N-terminal half adopting an extended conformation that is

INSTITUTO
DE INVESTIGAÇÃO
E INOVAÇÃO
EM SAÚDE
UNIVERSIDADE
DO PORTO

Rua Alfredo Allen, 208
4200-135 Porto
Portugal
+351 220 408 800
info@i3s.up.pt
www.i3s.up.pt

perpendicular to the helix. Interestingly, the conformation of BDC2 roughly resembles the one found in the structure of CaM bound to a fragment of the Orai1 channel (Liu et al., 2012). In the Ora1 structure the N-terminal half of the channel fragment is also in an extended conformation and the C-terminal half forms a helix. Just like in our structure, the two sections of the channel fragment are positioned at ~90º of each other and the helix lies on the cleft of the C-lobe of CaM. However, the fragments are in different orientations in the two structures, almost as mirror images of each other. An important point to consider about the CaM-BDC2 structure is whether the BDC2 conformation is a crystal artifact and bending of the channel fragment is the result of crystal lattice contacts between the N-terminal stretch and a neighboring CaM molecule. This issue is discussed in detail further down.

Based on data presented here and on previously published results we considered two models for the mechanism of CaM action: a model where CaM induces a global conformational change in the cytoplasmic regions of the channel and another where the effect of CaM is local. In both models the very tight interaction between the C-lobe of CaM and BDC2 is central for the mechanism of inhibition. The global conformation model is based on the fact that when CaM binds to BDC2 it leaves the N-lobe free to interact with other channel regions. It is therefore plausible to consider that, in the full-length channel, CaM binds to BDC2 through the C-lobe, while the N-lobe either interacts with BDN, bridging the N- and C-termini of the channel, or with another BDC2 site, bridging subunits. Our ITC and mass spectrometry analyses of the CNBh-BDC1-BDC2 channel fragment seem to rule out CaM-bridging of BDC2 and BDC1 and the 2:2 complex species identified by native mass spectrometry suggests that bridging of different subunits is possible. The affinity of the N-lobe for either BDN or BDC2 sites is low (K_D ~2-4 µM), however, a simple calculation for 4 BDN sites in a hemisphere volume with a radius of 200 Å (as a comparison the thickness of a lipid bilayer is ~50 Å) reveals local concentration values that are hundreds of times above K_D. Altogether this suggests a model where CaM bridges distant channel regions and induces a global conformational change that results in channel inhibition. Similar models have been proposed for the mechanisms of how voltage-gated Ca^{2+} channels (Ben Johny et al., 2013) or voltage-gated Na^{+} channels (Gabelli et al., 2014; Sarhan et al., 2012) are modulated by CaM.

The local conformation model emerges out of the previously published observation (Ziechner et al., 2006) that the mutant CaM-EF12 (where the N-lobe does not bind Ca^{2+}) is able to inhibit the hEAG1 channel, although with reduced potency: wild-type CaM at 270 nM reduced channel current to ~9%, while CaM-EF12 at a 4x higher concentration reduced the current to ~30%. In contrast, CaM-EF34 mutant (no Ca^{2+} binding at the C-lobe) did not inhibit the channel even at 1 µM. This result suggests that the interactions through the N-lobe are not required for inhibition and, therefore, that the mechanism of inhibition is not dependent on CaM bridging. This leads us to consider a model where inhibition results from a local conformational change induced by the C-lobe.

The bent conformation of the BDC2 channel fragment present in our CaM–BDC2 structure (Figure 2a and 2b) seems to provide evidence to support this model. However, the observation that the N-terminal stretch of BDC2 lies between crystallographically related CaM molecules (Figure 2c) together with the small impact in binding affinity of mutations in this section and in the elbow of BDC2 could be an indication that the bent conformation is a crystallographic artifact and that the N-terminal stretch is not relevant for the inhibition mechanism. Strikingly, we have found that mutations in the N-terminal stretch and elbow have a large functional effect. This is particularly evident in the alanine mutations at the two leucine residues in the N-terminal stretch (L702 and L704 in hEAG1 -

INSTITUTO
DE INVESTIGAÇÃO
E INOVAÇÃO
EM SAÚDE
UNIVERSIDADE
DO PORTO

Rua Alfredo Allen, 208
4200-135 Porto
Portugal
+351 220 408 800
info@i3s.up.pt
www.i3s.up.pt

red bar in Figure 3c) or at the aspartate and histidine residues positioned in the elbow of BDC2 (D707 and H708 in hEAG1 – cyan bar in Figure 3c). Moreover, a closer inspection of the thermodynamic parameters extracted from the ITC experiments reveals that these mutations, although not changing affinity, cause a clear change in binding enthalpy (by at least 5 kcal/mol) indicating that binding interactions have been altered by the mutations. Although we cannot rule out the possibility that the bent conformation of BDC2 is the result of contacts with the crystal lattice, the changes in binding enthalpy and functional impact associated with the mutants in the N-terminal section of BDC2 are consistent with the involvement of these residues in the interactions observed in the hydrophobic cluster (Figure 2d) and elbow (Figure 2e), which seem to stabilize the bent conformation.

The functional and biochemical mutagenesis results can be explained if the interaction between the C-lobe and BDC2 is dominated by the C-terminal BDC2 helix sitting on the cleft of the lobe, while the inhibitory effect requires the stabilization of the bent conformation in BDC2. Thus, in the local conformation model we propose that both the interaction with BDC2 and the stabilization of the bent conformation play a role in the inhibitory mechanism. In this model the "free" N-lobe of CaM still interacts with other regions of the channel, but these serve to further stabilize the local structural change induced by CaM increasing the potency of its inhibitory effect.

Our structural, biochemical and functional analysis of the CaM binding sites within the EAG1 channel suggests that the molecular change induced by CaM and underlying channel inhibition occurs locally. This appears to be very different from the mechanisms proposed for other tetrameric cation channels (Na^+ and Ca^{2+} channels) (Ben Johny et al., 2013; Gabelli et al., 2014; Sarhan et al., 2012) where CaM bridges sites in different regions of the channel giving rise to a global conformational change. It is interesting to notice, however, that in $Ca_V1.3$ the isolated CaM lobes also have an effect on channel function (Ben Johny et al., 2013). This means that bridging is not an absolute requirement for the mechanism of CaM in these channels and that local conformational changes play a role in these processes just like in EAG1 potassium channels. We still do not know how the CaM-induced change is reflected in channel inhibition and further studies will be necessary for a full understanding of the molecular mechanisms coupling CaM binding to conformational changes involved in channel opening.

INSTITUTO
DE INVESTIGAÇÃO
E INOVAÇÃO
EM SAÚDE
UNIVERSIDADE
DO PORTO

Rua Alfredo Allen, 208
4200-135 Porto
Portugal
+351 220 408 800
info@i3s.up.pt
www.i3s.up.pt

Experimental procedures

Expression and purification of protein constructs

Calmodulin binding sequences BDN and BDC2 from mEAG1 (accession codes NP_034730.1 and GI:6754422) were cloned into multiple cloning site 1 (MCS1) of modified pRSFDuet-1 (Novagen) which includes an N-terminal His_6-tag, maltose binding protein (MBP) and a TEV protease recognition sequence (HMT) at MCS1. Expression and purification of MBP fusions, calmodulin and channel fragments is described in SI and (Marques-Carvalho et al., 2012). CNBhD-BDC1 was prepared as described in (Marques-Carvalho et al., 2012).

Isothermal titration calorimetry

Titration components were dialyzed overnight against 50 mM Hepes pH 7.5, 150 mM NaCl, 5 mM $CaCl_2$, 1 mM TCEP (when necessary $CaCl_2$ was replaced by 5 mM EDTA) in the same beaker to avoid buffer mismatch. CaM concentration was determined by 277 nm absorbance (ε_{277nm}=3029 M^{-1} cm^{-1}) (Strasburg et al., 1988). Channel fragment concentration was determined by 280 nm absorbance using extinction coefficients calculated with ExPASy tool Protparam. CaM was degassed for 5 min before experiment. Titrations were performed at 25 ºC using a VP-ITC instrument (MicroCal), with a first injection of 2 µL, followed by 28x10 µL injections. Data were analyzed with MicroCal-Origin 7 or AFFINImeter. The first injection was ignored and correction for the heat of dilution was made by subtracting the average of the last four injection areas from all injection points.

Purification calmodulin-BDC2 complex for crystallization

The BDC2 MBP-fusion was co-expressed with CaM (cloned into MCS2 of pRSFDuet-1, without affinity tag). Preparation of the calmodulin-BDC2 complex is as for BDC2, except that buffers included 5 mM $CaCl_2$. Details in SI.

Crystallization, data collection, and refinement

Crystals were grown at 20 °C by sitting-drop and mixing a 1:1 (v/v) ratio of protein mixture with reservoir solution containing 0.2 M di-ammonium citrate pH 5, 20% PEG 3350. Data were collected at Proxima 2A beamline (Soleil Synchrotron) and were integrated and scaled using XDS (Kabsch, 2010) and Aimless (Evans and Murshudov, 2013) - CCP4 program suite (Winn et al., 2011). Structure was solved by molecular replacement with Phaser (McCoy et al., 2007) using ensembles of calmodulin N- and C-lobes as search models (PDB codes: 1CFD, 1CLL, 2BE6, 3DVM, 3OXQ chain A, 3OXQ chain B, 4DJC and 4GOW). Model was refined in PHENIX (Adams et al., 2010) with TLS (Painter and Merritt, 2006), built in Coot (Emsley and Cowtan, 2004) and figures created in PyMOL (DeLano, 2002).

Fluorescence anisotropy

PAS domain (mEAG1 1-137) was cloned in a pET15b vector. Expression and purification protocol is described in SI. Fluorescein labeling of PAS domain cysteines and binding assay are as described in SI and (Taraska et al., 2009; Haitin et al., 2013).

INSTITUTO
DE INVESTIGAÇÃO
E INOVAÇÃO
EM SAÚDE
UNIVERSIDADE
DO PORTO

Rua Alfredo Allen, 208
4200-135 Porto
Portugal
+351 220 408 800
info@i3s.up.pt
www.i3s.up.pt

Electrophysiology

Mutagenesis and mRNA synthesis were performed as in (Ziechner et al., 2006). For hEAG1 channel expression, stage V oocytes from *X. laevis* were injected with 50 nl of diluted mRNA. Ionic currents were recorded at 20-23 °C in two-electrode voltage clamp, using a Turbo-TEC 10CD amplifier (NPI electronic, Tamm, Germany) controlled by the PatchMaster software (HEKA Elektronik, Lambrecht, Germany); P/n leak correction was applied. Bath solution contained (in mM): 115 NaCl, 2.5 KCl, 1.8 CaCl2, 10 HEPES; pH 7.2 (NaOH). Ca^{2+} sensitivity was assessed using the ionophore ionomycin, applied during repetitive test pulses (from -120 mV to 40 mV; 400 ms) with 10 sec intervals. Control wash with bath solution (2 ml) was performed after 10 pulses. Ionomycin (1 µM in 2 ml bath solution) was added after 20^{th} pulse and washed out after pulse 60. Current amplitudes in test pulses were normalized to last pulse before ionomycin application and mean current reduction was evaluated for steady-state inhibition. Data were analyzed with FitMaster software (HEKA Elektronik) and IgorPro (WaveMetrics, Lake Oswego, OR, USA). Groups of data were compared with a two-sided student's t-test assuming unequal variances.

Native mass spectrometry

Protein samples were desalted by Micro gel filtration spin columns (7 kDa cut-off and with a bed volume of 75 µL- Zeba, Thermo Scientific) equilibrated with 100 mM ammonium acetate pH 7. Desalted samples were analyzed in native conditions by direct infusion in a 4-GHz MaXis ultra-high-resolution Q-TOF mass spectrometer from Bruker Daltonics (Germany) equipped with electrospray ion source.

Spectra were acquired in positive ion MS mode over a 1000–5500 m/z range with nebulizer gas pressure of 0.8 bars and spray voltage of –4 kV. Drying gas flow was 7 liter/min andtemperature120 °C. In source collision induced dissociation (isCID) parameter was adjusted at 100 eV to preserve noncovalent interactions of protein complex. Acquisition rate was 1 Hz corresponding to spectra summations of 4081. External calibration was performed with the ESI-L Low Concentration Tuning Mix (Agilent Technologies). Mass spectra were processed using DataAnalysis 3.1 software (Bruker Daltonics).

Accession numbers

Atomic coordinates and structure factors of calmodulin-BDC2 complex structure are deposited in the PDB under accession code PDB: 5HIT.

Author contributions

MJM-C and JHM-C designed the research. MJM-C performed the crystallography and ITC binding assays and together with EM and JHM-C analyzed the data. JO, SHH and RS designed and performed the electrophysiology experiments. ASF performed the fluorescence binding assay. GG and MC performed the mass spectrometry analysis. All authors reviewed and contributed to the manuscript.

Acknowledgments

INSTITUTO
DE INVESTIGAÇÃO
E INOVAÇÃO
EM SAÚDE
UNIVERSIDADE
DO PORTO

Rua Alfredo Allen, 208
4200-135 Porto
Portugal
+351 220 408 800
info@i3s.up.pt
www.i3s.up.pt

We are grateful for access to Proxima-2 at SOLEIL and the ESRF beamlines (through the Portuguese BAG). Work was financed by FEDER - Fundo Europeu de Desenvolvimento Regional funds through COMPETE 2020 - Operational Program for Competitiveness and Internationalization (POCI), Portugal 2020, and by Portuguese funds through FCT - Fundação para a Ciência e a Tecnologia/ Ministério da Ciência, Tecnologia e Inovação in the framework of the project "Institute for Research and Innovation in Health Sciences" (POCI-01-0145-FEDER-007274) and project FCOMP-01-0124-FEDER-028115 (PTDC/BBB-BQB/1418/2012), and by National Institutes of Health - NS081320, European FEDER grant #2699-33931 and Region Centre grant SyMBioMS. Conflict of interest declaration: Eva Muñoz is an employee and shareholder of AFFINImeter. All other authors declare no conflict of interest.

References

Adaixo, R., Harley, C.A., Castro-Rodrigues, A.F., and Morais-Cabral, J.H. (2013). Structural properties of PAS domains from the KCNH potassium channels. PLoS One *8*, e59265.

Adams, P.D., Afonine, P.V., Bunkoczi, G., Chen, V.B., Davis, I.W., Echols, N., Headd, J.J., Hung, L.W., Kapral, G.J., Grosse-Kunstleve, R.W., *et al.* (2010). PHENIX: a comprehensive Python-based system for macromolecular structure solution. Acta Crystallogr D Biol Crystallogr *66*, 213-221.

Ben Johny, M., Yang, P.S., Bazzazi, H., and Yue, D.T. (2013). Dynamic switching of calmodulin interactions underlies Ca2+ regulation of CaV1.3 channels. Nat Commun *4*, 1717.

Cherubini, A., Hofmann, G., Pillozzi, S., Guasti, L., Crociani, O., Cilia, E., Di Stefano, P., Degani, S., Balzi, M., Olivotto, M., *et al.* (2005). Human ether-a-go-go-related gene 1 channels are physically linked to beta1 integrins and modulate adhesion-dependent signaling. Mol Biol Cell *16*, 2972-2983.

Crociani, O., Guasti, L., Balzi, M., Becchetti, A., Wanke, E., Olivotto, M., Wymore, R.S., and Arcangeli, A. (2003). Cell cycle-dependent expression of HERG1 and HERG1B isoforms in tumor cells. J Biol Chem *278*, 2947-2955.

DeLano, W.L. (2002). The PyMOL Molecular Graphics System, Schrödinger, LLC. .

Emsley, P., and Cowtan, K. (2004). Coot: model-building tools for molecular graphics. Acta Crystallogr D Biol Crystallogr *60*, 2126-2132.

Evans, P.R., and Murshudov, G.N. (2013). How good are my data and what is the resolution? Acta Crystallogr D Biol Crystallogr *69*, 1204-1214.

Fernandes, A.S., Morais-Cabral, J.H., and Harley, C.A. (2016). Screening for Non-Pore-Binding Modulators of EAG K+ Channels. J Biomol Screen.

Gabelli, S.B., Boto, A., Kuhns, V.H., Bianchet, M.A., Farinelli, F., Aripirala, S., Yoder, J., Jakoncic, J., Tomaselli, G.F., and Amzel, L.M. (2014). Regulation of the NaV1.5 cytoplasmic domain by calmodulin. Nat Commun *5*, 5126.

Goncalves, J.T., and Stuhmer, W. (2010). Calmodulin interaction with hEAG1 visualized by FRET microscopy. PLoS One *5*, e10873.

Grabarek, Z. (2005). Structure of a trapped intermediate of calmodulin: calcium regulation of EF-hand proteins from a new perspective. J Mol Biol *346*, 1351-1366.

INSTITUTO
DE INVESTIGAÇÃO
E INOVAÇÃO
EM SAÚDE
UNIVERSIDADE
DO PORTO

Rua Alfredo Allen, 208
4200-135 Porto
Portugal
+351 220 408 800
info@i3s.up.pt
www.i3s.up.pt

Gustina, A.S., and Trudeau, M.C. (2011). hERG potassium channel gating is mediated by N- and C-terminal region interactions. J Gen Physiol *137*, 315-325.

Haitin, Y., Carlson, A.E., and Zagotta, W.N. (2013). The structural mechanism of KCNH-channel regulation by the eag domain. Nature *501*, 444-448.

Kabsch, W. (2010). Integration, scaling, space-group assignment and post-refinement. Acta Crystallogr D Biol Crystallogr *66*, 133-144.

Krissinel, E., and Henrick, K. (2004). Secondary-structure matching (SSM), a new tool for fast protein structure alignment in three dimensions. Acta Crystallogr D Biol Crystallogr *60*, 2256-2268.

Liu, Y., Zheng, X., Mueller, G.A., Sobhany, M., DeRose, E.F., Zhang, Y., London, R.E., and Birnbaumer, L. (2012). Crystal structure of calmodulin binding domain of orai1 in complex with Ca2+ calmodulin displays a unique binding mode. J Biol Chem *287*, 43030-43041.

Lorinczi, E., Helliwell, M., Finch, A., Stansfeld, P.J., Davies, N., Mahaut-Smith, M., Muskett, F.W., and Mitcheson, J.S. (2016). Calmodulin regulates human ether a go-go 1 (hEAG1) potassium channels through interactions of the eag-domain with the cyclic nucleotide binding homology domain. J Biol Chem.

Marques-Carvalho, M.J., Sahoo, N., Muskett, F.W., Vieira-Pires, R.S., Gabant, G., Cadene, M., Schonherr, R., and Morais-Cabral, J.H. (2012). Structural, biochemical, and functional characterization of the cyclic nucleotide binding homology domain from the mouse EAG1 potassium channel. J Mol Biol *423*, 34-46.

McCoy, A.J., Grosse-Kunstleve, R.W., Adams, P.D., Winn, M.D., Storoni, L.C., and Read, R.J. (2007). Phaser crystallographic software. J Appl Crystallogr *40*, 658-674.

Morais-Cabral, J.H., and Robertson, G.A. (2015). The enigmatic cytoplasmic regions of KCNH channels. J Mol Biol *427*, 67-76.

Morgan, A.J., and Jacob, R. (1994). Ionomycin enhances Ca2+ influx by stimulating store-regulated cation entry and not by a direct action at the plasma membrane. Biochem J *300 (Pt 3)*, 665-672.

Painter, J., and Merritt, E.A. (2006). Optimal description of a protein structure in terms of multiple groups undergoing TLS motion. Acta Crystallogr D Biol Crystallogr *62*, 439-450.

Pardo, L.A., and Stuhmer, W. (2014). The roles of K(+) channels in cancer. Nat Rev Cancer *14*, 39-48.

Sahoo, N., Troger, J., Heinemann, S.H., and Schonherr, R. (2010). Current inhibition of human EAG1 potassium channels by the Ca2+ binding protein S100B. FEBS Lett *584*, 3896-3900.

Sanguinetti, M.C., and Tristani-Firouzi, M. (2006). hERG potassium channels and cardiac arrhythmia. Nature *440*, 463-469.

Sarhan, M.F., Tung, C.C., Van Petegem, F., and Ahern, C.A. (2012). Crystallographic basis for calcium regulation of sodium channels. Proc Natl Acad Sci U S A *109*, 3558-3563.

Schonherr, R., Lober, K., and Heinemann, S.H. (2000). Inhibition of human ether a go-go potassium channels by Ca(2+)/calmodulin. EMBO J *19*, 3263-3271.

INSTITUTO
DE INVESTIGAÇÃO
E INOVAÇÃO
EM SAÚDE
UNIVERSIDADE
DO PORTO

Rua Alfredo Allen, 208
4200-135 Porto
Portugal
+351 220 408 800
info@i3s.up.pt
www.i3s.up.pt

Strasburg, G.M., Hogan, M., Birmachu, W., Thomas, D.D., and Louis, C.F. (1988). Site-specific derivatives of wheat germ calmodulin. Interactions with troponin and sarcoplasmic reticulum. J Biol Chem *263*, 542-548.

Sun, X.X., Hodge, J.J., Zhou, Y., Nguyen, M., and Griffith, L.C. (2004). The eag potassium channel binds and locally activates calcium/calmodulin-dependent protein kinase II. J Biol Chem *279*, 10206-10214.

Taraska, J.W., Puljung, M.C., Olivier, N.B., Flynn, G.E., and Zagotta, W.N. (2009). Mapping the structure and conformational movements of proteins with transition metal ion FRET. Nat Methods *6*, 532-537.

Wang, Z., Wilson, G.F., and Griffith, L.C. (2002). Calcium/calmodulin-dependent protein kinase II phosphorylates and regulates the Drosophila eag potassium channel. J Biol Chem *277*, 24022-24029.

Warmke, J.W., and Ganetzky, B. (1994). A family of potassium channel genes related to eag in Drosophila and mammals. Proc Natl Acad Sci U S A *91*, 3438-3442.

Winn, M.D., Ballard, C.C., Cowtan, K.D., Dodson, E.J., Emsley, P., Evans, P.R., Keegan, R.M., Krissinel, E.B., Leslie, A.G., McCoy, A., *et al.* (2011). Overview of the CCP4 suite and current developments. Acta Crystallogr D Biol Crystallogr *67*, 235-242.

Yamniuk, A.P., and Vogel, H.J. (2004). Calmodulin's flexibility allows for promiscuity in its interactions with target proteins and peptides. Mol Biotechnol *27*, 33-57.

Yao, Y., and Tsien, R.Y. (1997). Calcium current activated by depletion of calcium stores in Xenopus oocytes. J Gen Physiol *109*, 703-715.

Yoshida, S., and Plant, S. (1992). Mechanism of release of Ca2+ from intracellular stores in response to ionomycin in oocytes of the frog Xenopus laevis. J Physiol *458*, 307-318.

Ziechner, U., Schonherr, R., Born, A.K., Gavrilova-Ruch, O., Glaser, R.W., Malesevic, M., Kullertz, G., and Heinemann, S.H. (2006). Inhibition of human ether a go-go potassium channels by Ca2+/calmodulin binding to the cytosolic N- and C-termini. FEBS J *273*, 1074-1086.

INSTITUTO
DE INVESTIGAÇÃO
E INOVAÇÃO
EM SAÚDE
UNIVERSIDADE
DO PORTO

Rua Alfredo Allen, 208
4200-135 Porto
Portugal
+351 220 408 800
info@i3s.up.pt
www.i3s.up.pt

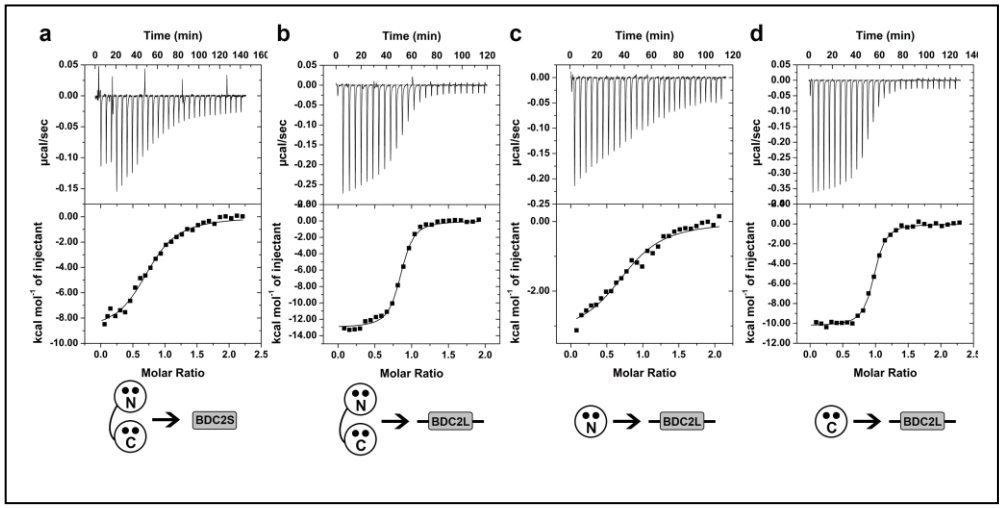

Figure 1: Characterization of the interaction of CaM with BDC2. a) ITC titration of 60 µM CaM into 6 µM MBP-BDC2S. **b)** Titration of 60 µM CaM into 6 µM MBP-BDC2L. **c)** Titration of 180 µM N-lobe CaM into 19 µM MBP-BDC2L. **d)** Titration of 100 µM C-lobe CaM into 10 µM MBP-BDC2L. Top graphs show heat power changes, bottom graphs show integrated heat values fitted with a model curve. Cartoons represent components in each titration with CaM lobes (N- and C-, as labeled) shown as circles, full-length CaM represented by linked circles, Ca^{2+} bound in lobes shown as closed dots, lobes without Ca^{2+} have no dots. Experiments performed in saturating Ca^{2+} concentrations (5 mM).

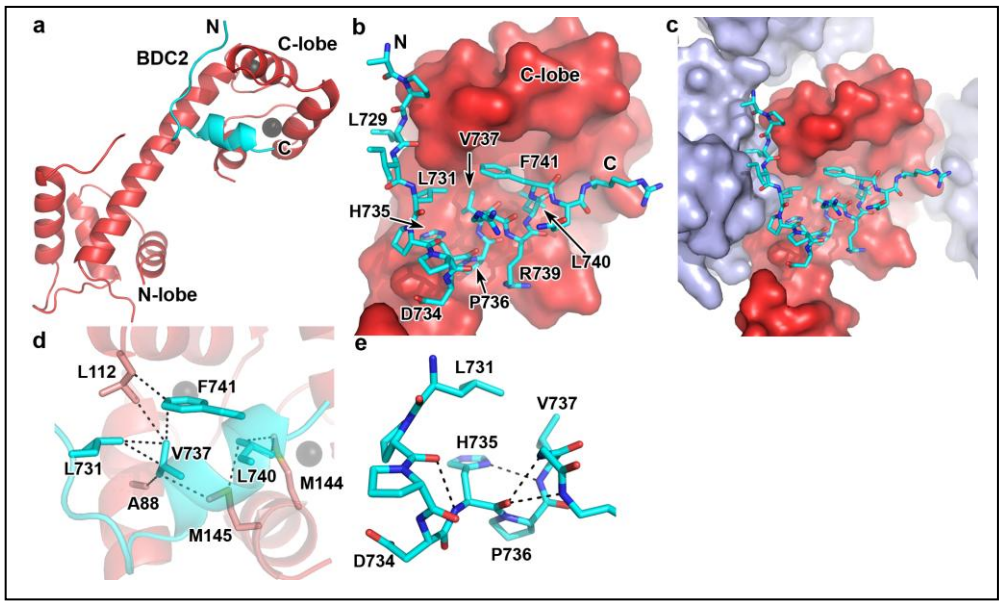

Figure 2: Structure of calmodulin in complex with BDC2. a) Full view of Ca^{2+}-CaM-BDC2 structure with CaM in red cartoon and BDC2 in cyan. Calcium ions are represented by black spheres. **b)** Zoom over the C-lobe (shown as surface) and BDC2 channel fragment (in stick). **c)** View of the crystal lattice with neighboring CaM molecules in lilac. **d)** View of residues in hydrophobic cluster. Only side-chains are shown, cyan for BDC2 and red for CaM. Van der Waals contacts (≤ 4 Å) shown as dashed lines. Ca^{2+} shown as spheres. **e)** View of residues in elbow of BDC2 with potential hydrogen bond network (donor and acceptor at ≤ 3.5 Å) shown as dashed lines.

INSTITUTO
DE INVESTIGAÇÃO
E INOVAÇÃO
EM SAÚDE
UNIVERSIDADE
DO PORTO

Rua Alfredo Allen, 208
4200-135 Porto
Portugal
+351 220 408 800
info@i3s.up.pt
www.i3s.up.pt

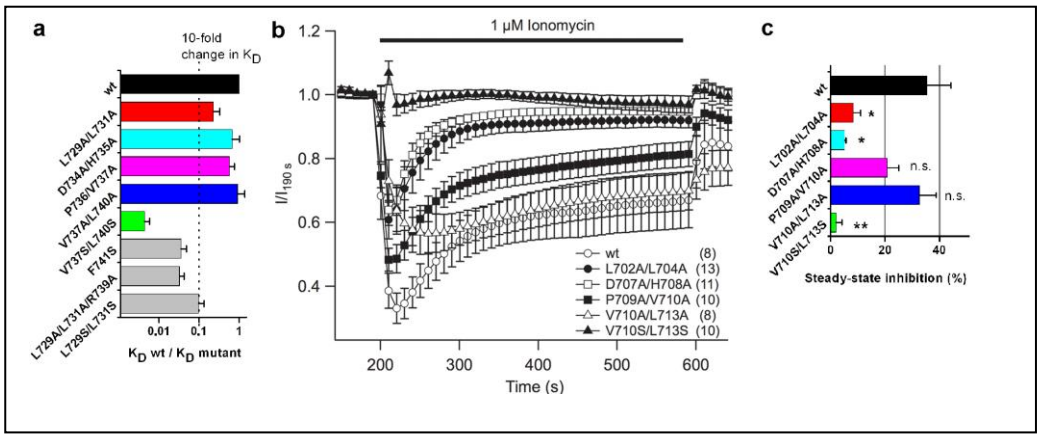

Figure 3: Characterization of BDC2 mutants. a) Dissociation constant ratios for wild type CaM-BDC2 complex relative to mutants. **b)** Time course of normalized current inhibition after elevation of intracellular Ca^{2+} by extracellular exposure to 1 µM ionomycin. Wild-type and mutant hEAG1 channels were expressed in *Xenopus* oocytes and currents were recorded in two-electrode voltage clamp. Averaged currents during repetitive test pulses (40 mV) were normalized to current amplitudes before exposure to ionomycin. Numbers of independent experiments are in parentheses. **c)** Quantification of steady-state inhibition seen in b). Errors are SEM. Equivalent mutations are shown as bars of the same color in a) and c).

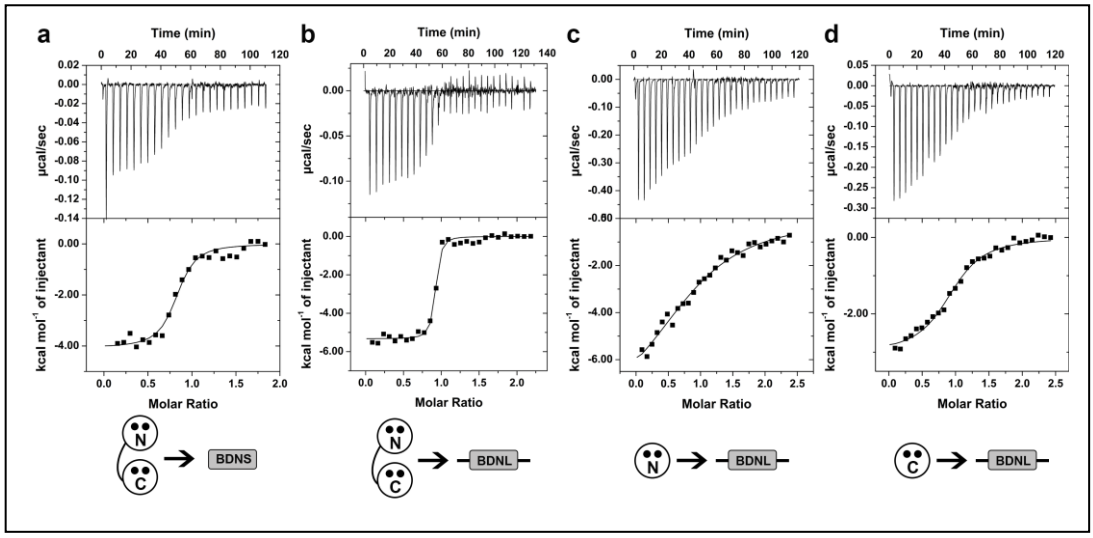

Figure 4: Characterization of the interaction of calmodulin with BDN. a) ITC titration of 60 µM CaM into 6 µM MBP- BDNS. **b)** Titration of 60 µM CaM into 6 µM MBP-BDNL. **c)** Titration of 253 µM N-lobe into 23 µM MBP-BDNL. **d)** Titration of 258 µM C-lobe into 23 µM MBP-BDNL. Organization of panels and symbols as in Figure 1. Experiments performed in saturating Ca^{2+} concentrations (5 mM).

INSTITUTO
DE INVESTIGAÇÃO
E INOVAÇÃO
EM SAÚDE
UNIVERSIDADE
DO PORTO

Rua Alfredo Allen, 208
4200-135 Porto
Portugal
+351 220 408 800
info@i3s.up.pt
www.i3s.up.pt

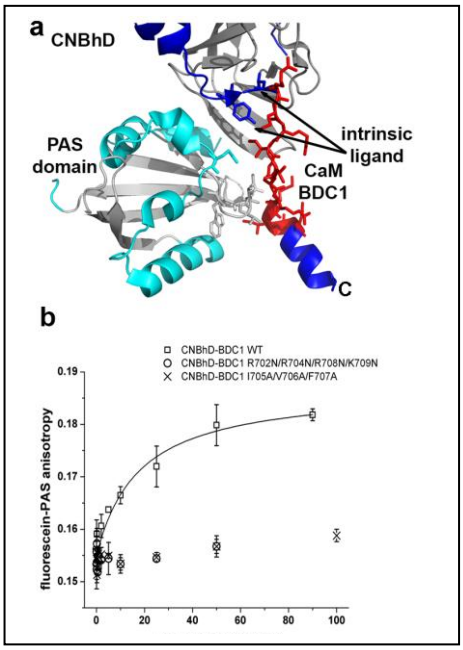

Figure 5: BDC1 mutations affect interaction between PAS and CNBh domains. a) Interface of complex formed by mEAG1 PAS (cyan and grey) and CNBhD-BDC1 (blue and grey) (Haitin et al., 2013). C terminus of CNBhD-BDC1 corresponds to either residue 717, 718 or 720 depending of which of the 4 complexes present in the crystal structure (PDB 4LLO) is analyzed. Intrinsic ligand residues in CNBh domain are shown; BDC1 region and residues in PAS domain that interact with BDC1 depicted in stick. **b)** Fluorescence anisotropy of fluorescein-labeled PAS domain titrated with wild-type CNBhD-BDC1 (squares) and with same protein mutated in the BDC1 region: R702N/R704N/R708N/K709N (circles) and I705A/V706A/F707A (crosses).

INSTITUTO
DE INVESTIGAÇÃO
E INOVAÇÃO
EM SAÚDE
UNIVERSIDADE
DO PORTO

Rua Alfredo Allen, 208
4200-135 Porto
Portugal
+351 220 408 800
info@i3s.up.pt
www.i3s.up.pt

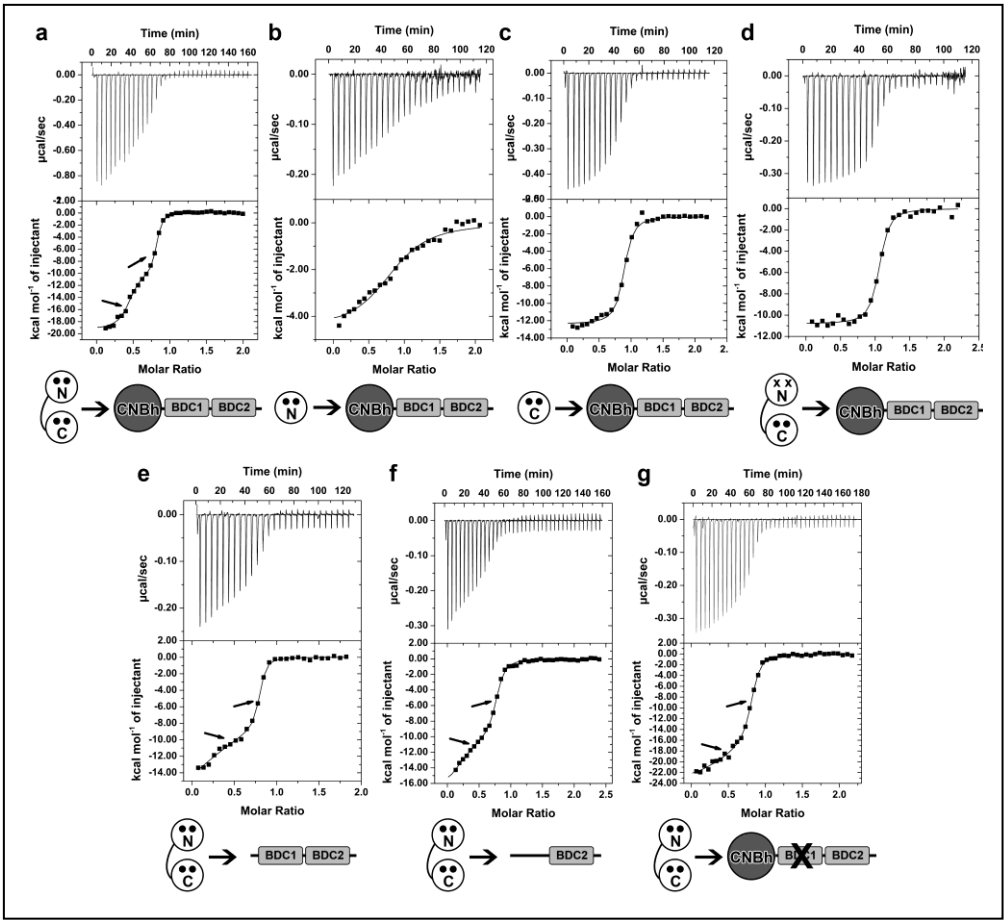

Figure 6: Characterization of the interaction of calmodulin with CNBhD-BDC1-BDC2. a) ITC titration of 187 µM CaM into 17 µM CNBhD-BDC1-BDC2, fitted with model considering two sets of independent sites on the channel fragment. **b)** Titration of 140 µM N-lobe into 14 µM CNBhD-BDC1-BDC2. **c)** Titration of 100 µM C-lobe into 10 µM CNBhD-BDC1-BDC2. **d)** Titration of 100 µM CaM-EF12 into 100 µM CNBhD-BDC1-BDC2. **e)** Titration of 60 µM CaM into 6 µM MBP-BDC1-BDC2, fitted as in a). **f)** Titration of 70 µM CaM into 6 µM MBP-linkerBDC2, fitted as in a). **g)** Titration of 60 µM CaM into 6 µM CNBhD-BDC1-BDC2 BDC1 mutant R702N/R704N/R708N/K709N, fitted as in a). Arrows indicate steps in binding isotherms. Organization of panels and symbols as in Figure 1; mutated Ca^{2+}-binding sites shown as small x, large X indicates mutations in BDC1. Experiments performed in saturating Ca^{2+} concentrations (5 mM).

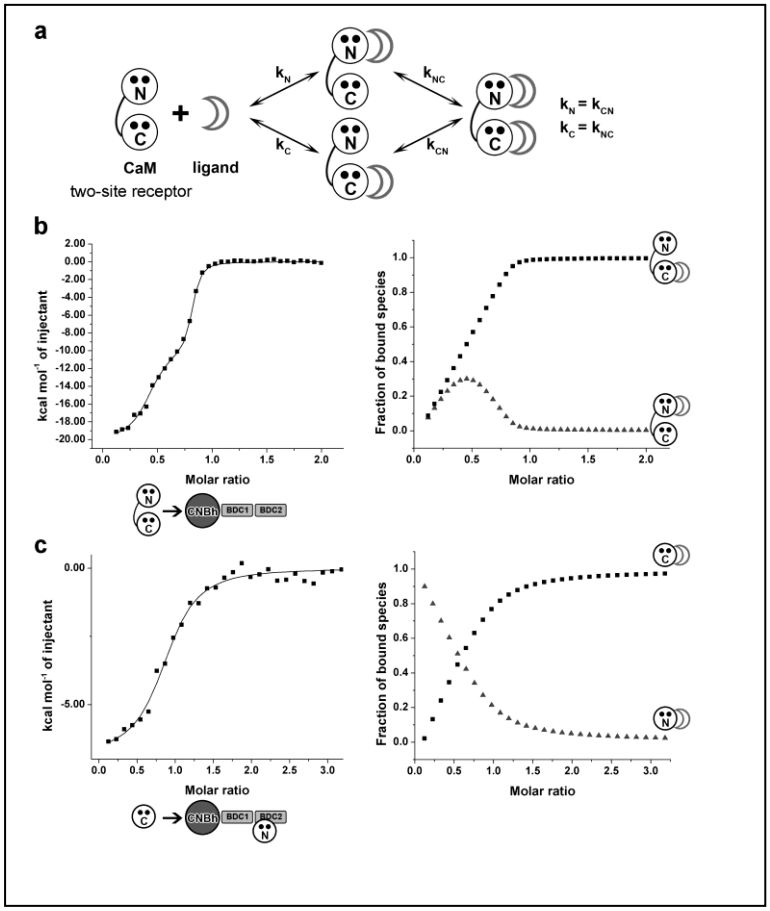

Figure 7: Modeling of calmodulin binding to CNBh-BDC1-BDC2. **a)** CaM independent-site binding model. k represents site-specific binding constants for each lobe (N- or C-). Cartoons as in Figure 1. **b)** Titration of 187 µM CaM into 17 µM CNBhD-BDC1-BDC2 (same data as in Figure 5a) fitted with model shown in a), together with respective species distribution plot. **c)** Titration of 100 µM C-lobe into a mixture of 7 µM CNBhD-BDC1-BDC2 and 35 µM N-lobe and species distribution plot. All experiments performed in saturating Ca^{2+} concentrations (5 mM).

INSTITUTO
DE INVESTIGAÇÃO
E INOVAÇÃO
EM SAÚDE
UNIVERSIDADE
DO PORTO

Rua Alfredo Allen, 208
4200-135 Porto
Portugal
+351 220 408 800
info@i3s.up.pt
www.i3s.up.pt

Supplemental Information:

It includes eight supplemental figures. It also includes Supplemental Experimental Procedures and Supplemental references.

INSTITUTO
DE INVESTIGAÇÃO
E INOVAÇÃO
EM SAÚDE
UNIVERSIDADE
DO PORTO

Rua Alfredo Allen, 208
4200-135 Porto
Portugal
+351 220 408 800
info@i3s.up.pt
www.i3s.up.pt

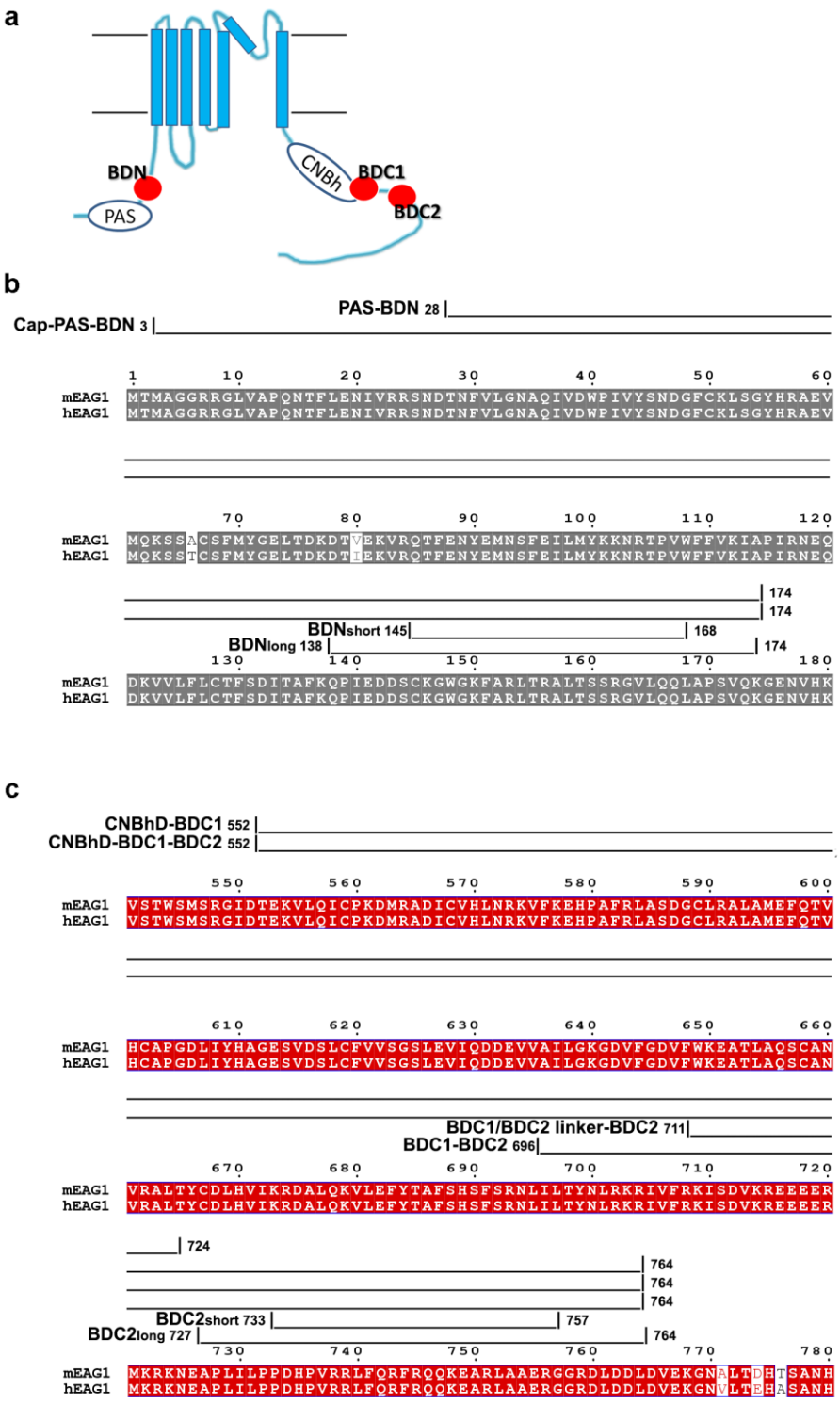

Figure S1, related to Figures 1, 4, 5 and 6: The EAG1 channel and its cytosolic regions. a) Cartoon representation of EAG1 channel subunit, with CaM binding sites and cytosolic globular domains shown. Amino acid sequence of b) N-terminal and c) C-terminal EAG1 channel cytosolic regions and limits of constructs used in this study.

INSTITUTO DE INVESTIGAÇÃO E INOVAÇÃO EM SAÚDE
UNIVERSIDADE DO PORTO

Rua Alfredo Allen, 208
4200-135 Porto
Portugal
+351 220 408 800
info@i3s.up.pt
www.i3s.up.pt

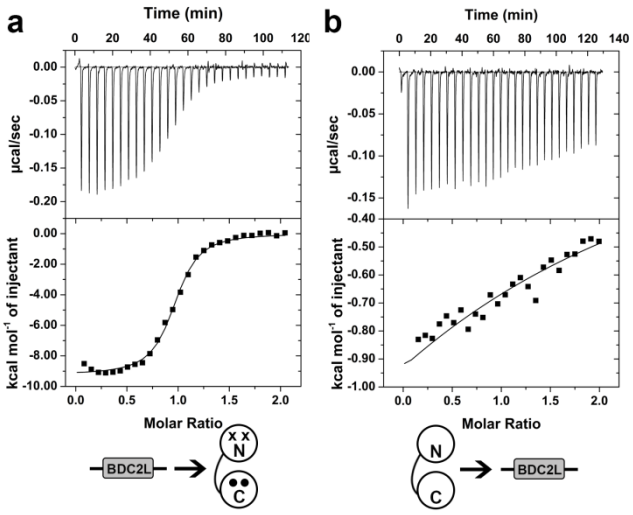

Figure S2, related to Figure 1: Titrations of BDC2 with Ca^{2+}-CaM EF12 mutant and with full-length CaM in the absence of Ca^{2+}. a) ITC titration of 60 µM MBP-$BDC2^{long}$ into 6 µM Ca^{2+}-CaM EF12 mutant. b) Titration of 500 µM apo-CaM into 50 µM MBP-$BDC2^{long}$ in the presence of 5 mM EDTA and at 25 ºC. Top graphs show heat power changes during injections, while bottom parts show the integrated heat values fitted with a model curve. Cartoons represent the components in each titration with CaM lobes (N- and C-, as labeled) shown as circles, full-length CaM represented by linked circles, Ca^{2+} bound in lobes shown as closed dots (lobes without bound Ca^{2+} have no dots).

INSTITUTO
DE INVESTIGAÇÃO
E INOVAÇÃO
EM SAÚDE
UNIVERSIDADE
DO PORTO

Rua Alfredo Allen, 208
4200-135 Porto
Portugal
+351 220 408 800
info@i3s.up.pt
www.i3s.up.pt

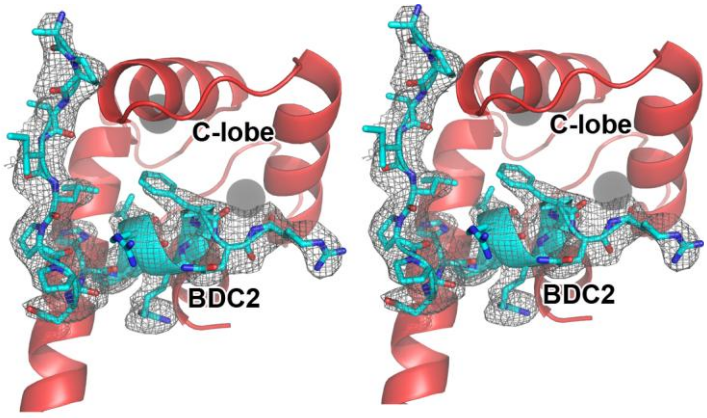

Figure S3, related to Figure 2: Stereo-view of the BDC2 channel fragment (shown as stick) bound to the C-lobe of CaM (red cartoon). 2Fobs-Fc map is shown as a mesh surrounding the BDC2.

INSTITUTO
DE INVESTIGAÇÃO
E INOVAÇÃO
EM SAÚDE
UNIVERSIDADE
DO PORTO

Rua Alfredo Allen, 208
4200-135 Porto
Portugal
+351 220 408 800
info@i3s.up.pt
www.i3s.up.pt

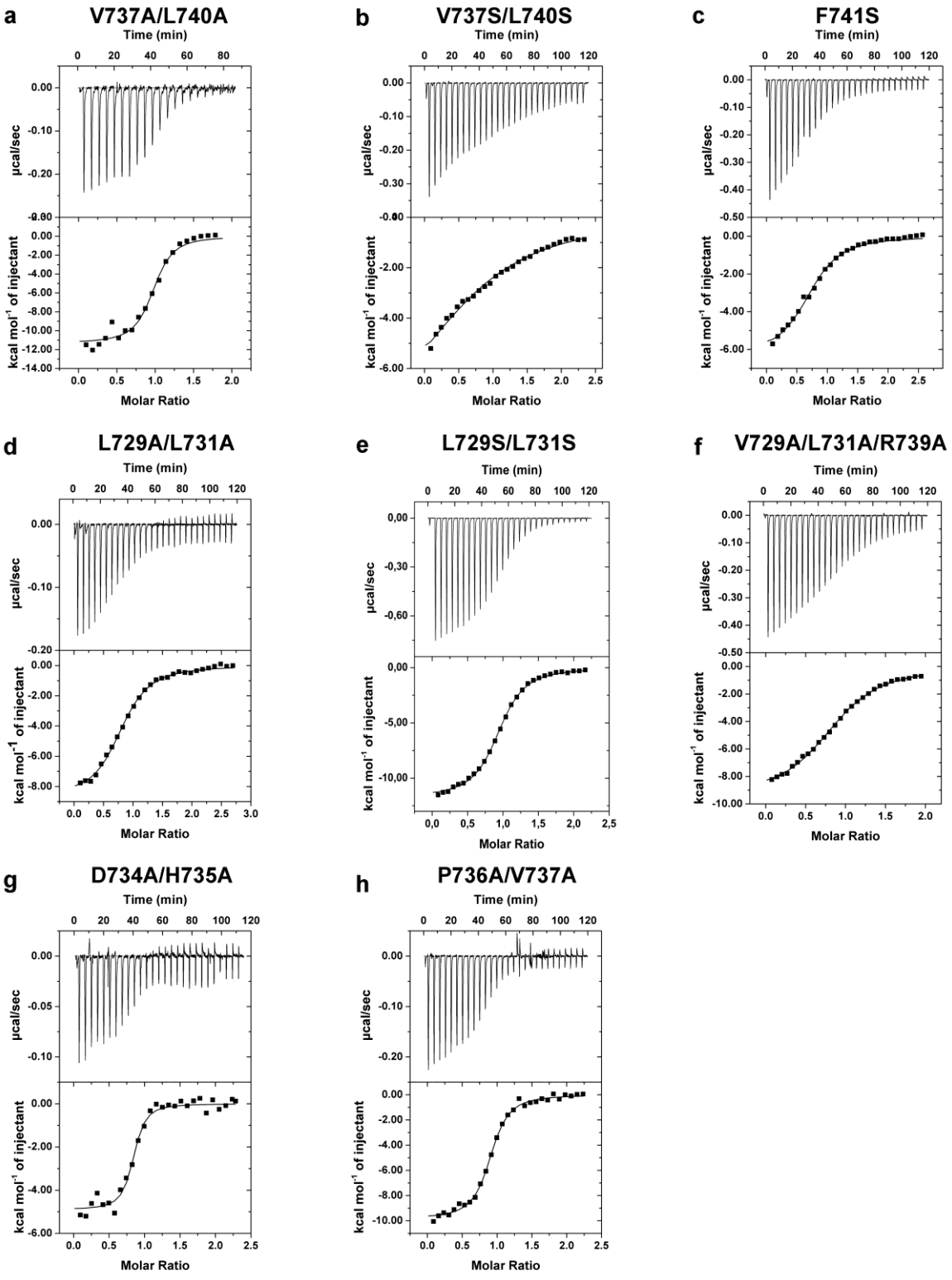

Figure S4, related to Figure 3.Titrations of BDC2 mutants with Ca^{2+}-CaM. Representative ITC titrations for each mutant; top graphs show heat power changes during injections, while bottom parts show the integrated heat values fitted with a model curve.

INSTITUTO
DE INVESTIGAÇÃO
E INOVAÇÃO
EM SAÚDE
UNIVERSIDADE
DO PORTO

Rua Alfredo Allen, 208
4200-135 Porto
Portugal
+351 220 408 800
info@i3s.up.pt
www.i3s.up.pt

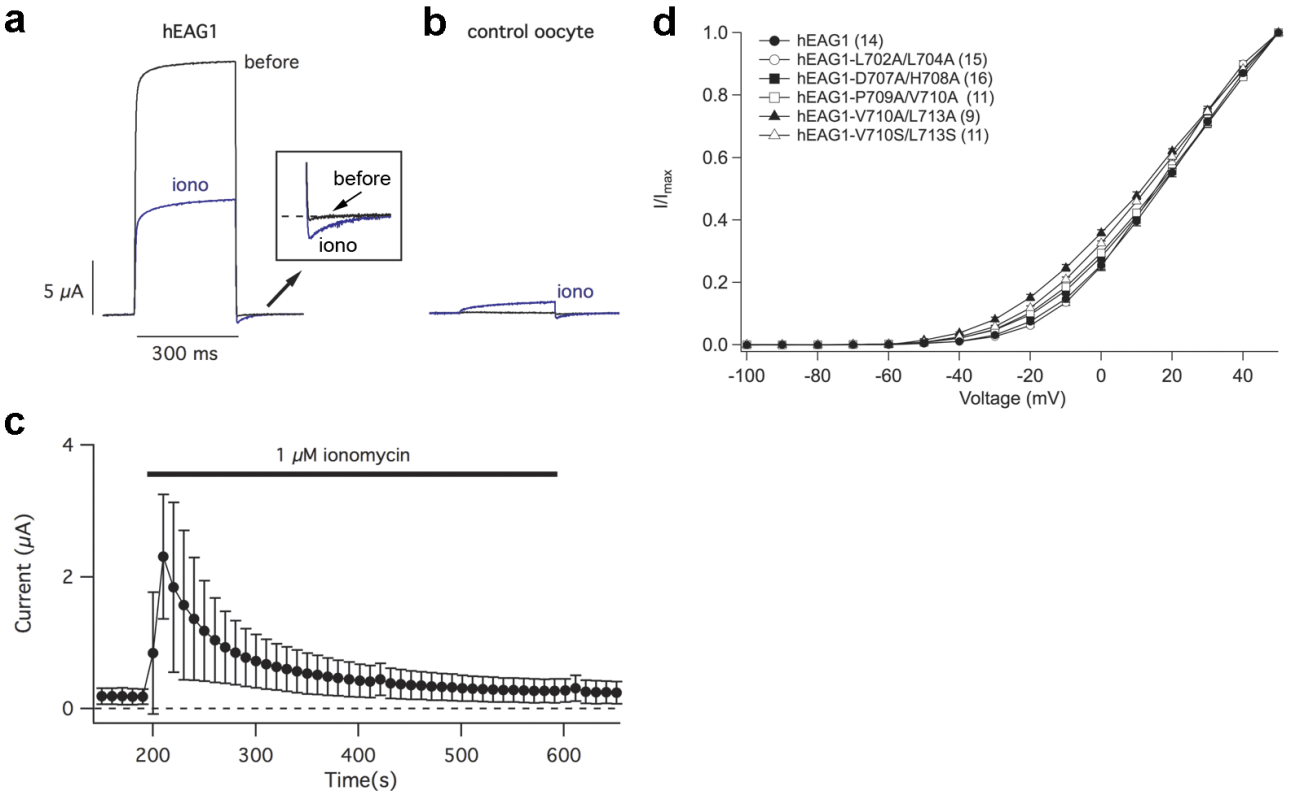

Figure S5, related to Figure 3: Endogenous current induced by ionomycin and current-voltage relationship of hEAG1 and BDC2 mutants. Representative current responses from two-electrode voltage clamp experiments measured in frog oocytes. Repetitive test pulses (300 ms) to +40 mV were applied every 10 s. The last current trace before treatment and the second trace in the presence of 1 µM ionomycin are shown for a) hEAG1 and b) for a water-injected oocyte. The inset in a) shows the tail currents in larger magnification. c) Mean endogenous current amplitudes from ionomycin-treated control cells (n=5); errors are SD. d) Normalized steady-state currents plotted versus depolarization voltages for wild type and BDC2 mutants. Depolarizing test pulses (2 s) ranged from -100 mV to +50 mV in steps of 10 mV and The numbers of experiments are given in parentheses; errors are SEM.

INSTITUTO
DE INVESTIGAÇÃO
E INOVAÇÃO
EM SAÚDE
UNIVERSIDADE
DO PORTO

Rua Alfredo Allen, 208
4200-135 Porto
Portugal
+351 220 408 800
info@i3s.up.pt
www.i3s.up.pt

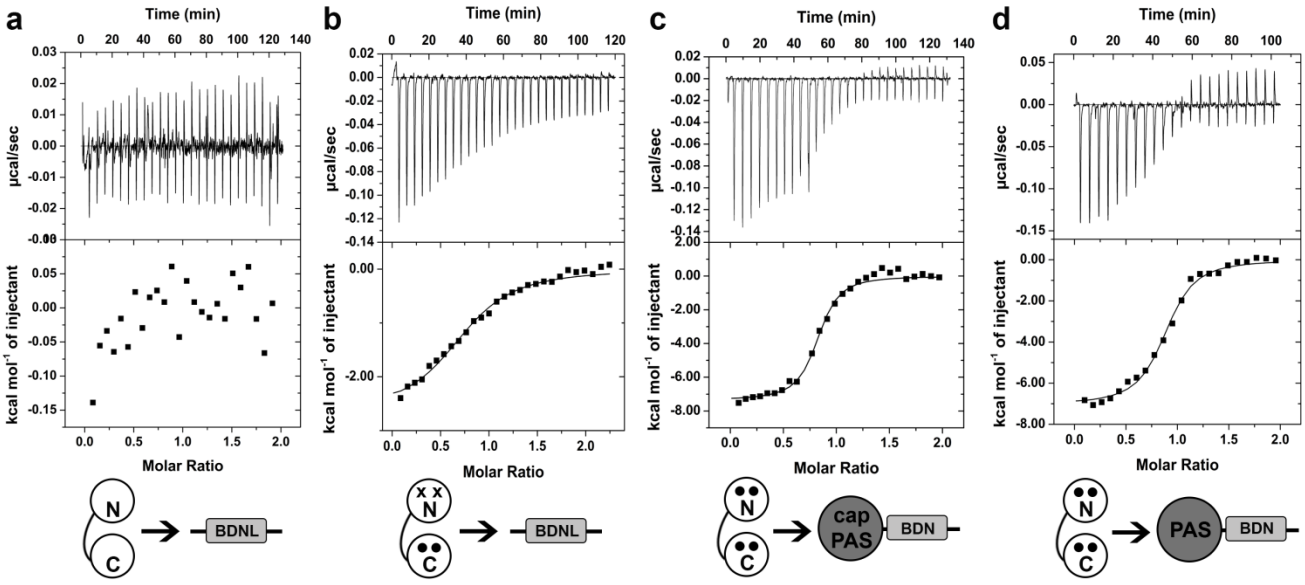

Figure S6, related to Figure 4: BDN interactions. a) ITC titration of 500 µM apo-CaM into 50 µM MBP-BDN^{long}, in the presence of 5 mM EDTA. b) ITC titration of 135 µM Ca^{2+}-CaM EF12 mutant into 13 µM MBP-BDN^{long}. c) ITC titration of 60 µM Ca^{2+}-CaM into 6 µM Cap-PAS-BDN. d) ITC titration of 60 µM Ca^{2+}-CaM into 6 µM PAS-BDN. Top graphs show heat power changes during injections, while bottom parts show the integrated heat values fitted with a model curve. Cartoons represent the components in each titration with CaM lobes (N- and C-, as labeled) shown as circles, full-length CaM represented by linked circles, Ca^{2+} bound in lobes shown as closed dots (lobes without bound Ca^{2+} have no dots) and mutated Ca^{2+}-binding sites shown as x.

INSTITUTO
DE INVESTIGAÇÃO
E INOVAÇÃO
EM SAÚDE
UNIVERSIDADE
DO PORTO

Rua Alfredo Allen, 208
4200-135 Porto
Portugal
+351 220 408 800
info@i3s.up.pt
www.i3s.up.pt

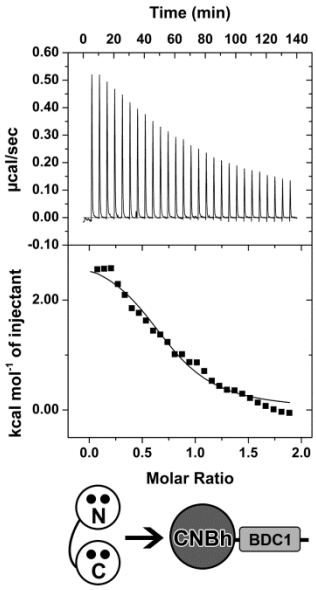

Figure S7, related to Figure 5: ITC titration of 500 µM Ca^{2+}-CaM into 50 µM CNBhD-BDC1. Top graph shows heat power changes during injections, while bottom part shows the integrated heat values fitted with a model curve. Cartoon represents the components in the titration with full-length CaM represented by two linked circles (N- and C-lobes, as indicated) with bound Ca^{2+} (closed dots).

INSTITUTO
DE INVESTIGAÇÃO
E INOVAÇÃO
EM SAÚDE
UNIVERSIDADE
DO PORTO

Rua Alfredo Allen, 208
4200-135 Porto
Portugal
+351 220 408 800
info@i3s.up.pt
www.i3s.up.pt

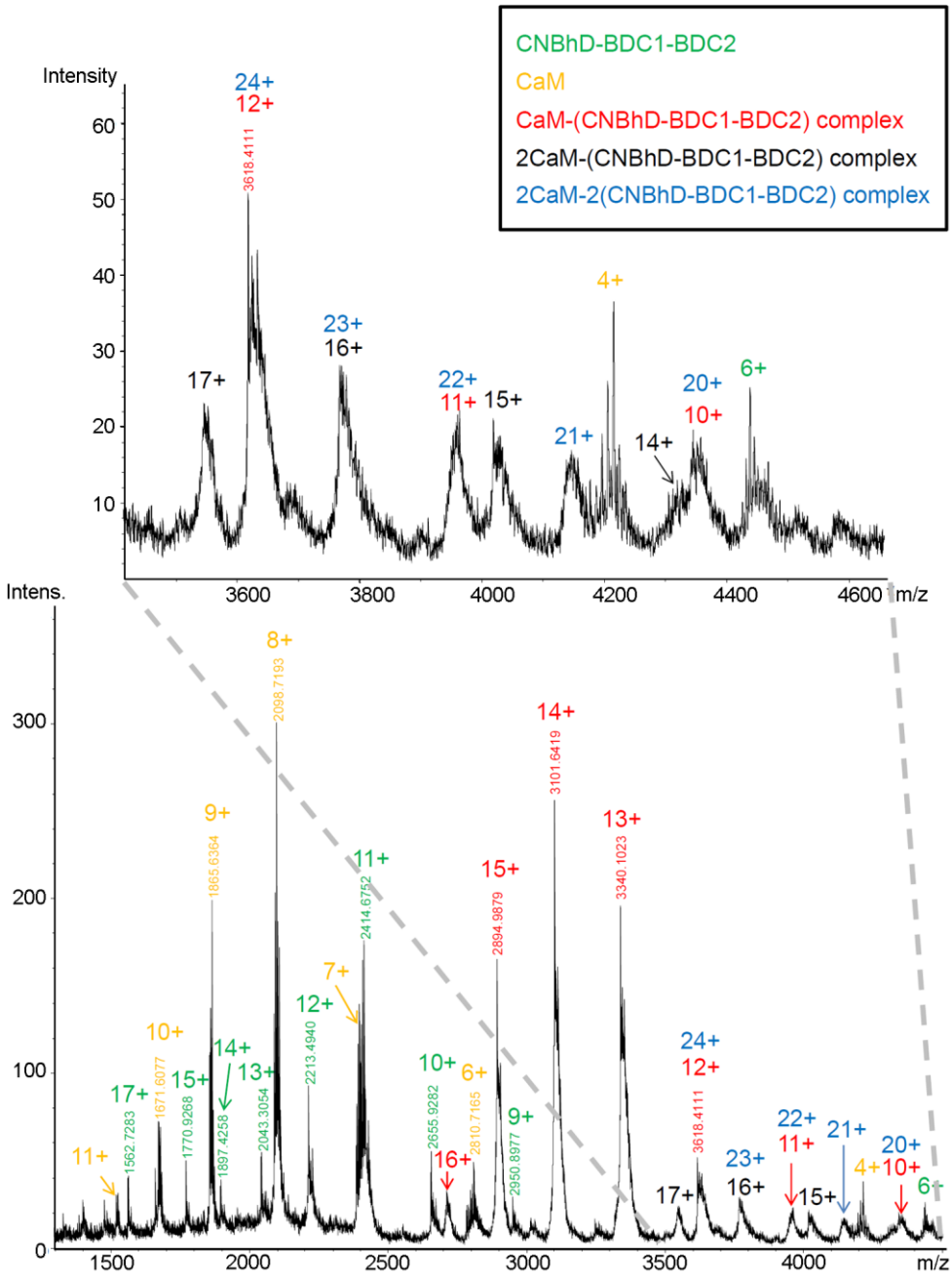

Figure S8, related to Figures 6: Native UHR-QTOF mass spectrum of CaM-(CNBhD-BDC1-BDC2) complexes. The mEAG CNBhD-BDC1-BDC2 domain in complex with calmodulin in a 1:1 ratio containing 1mM Ca^{2+} were desalted into a solution of ammonium acetate, 100 mM, pH 7.0 and analyzed by ultra-high resolution QTOF MS using direct infusion. The analyzed sample contains Ca^{2+} associated with the protein. Assigned identity of species present in the spectra is indicated. The 2:2 CaM:CNBhD-BDC1-BDC2 complex is distinguishable from the 1:1 complex through its odd-charged species and explains a peak, marked with blue "21+", which is not accounted by the other complexes.

Supplemental Experimental Procedures:

INSTITUTO
DE INVESTIGAÇÃO
E INOVAÇÃO
EM SAÚDE
UNIVERSIDADE
DO PORTO

Rua Alfredo Allen, 208
4200-135 Porto
Portugal
+351 220 408 800
info@i3s.up.pt
www.i3s.up.pt

Purification of MBP fusions

Pellets of cells expressing MBP fusions were resuspended in buffer A (50 mM HEPES pH 7.5, 250 mM KCl) supplemented with protease inhibitors. Cell lysis was performed in a cooled cell cracker (Emulsiflex-C5, Avestin) and the lysate was centrifuged at 32 800xg for 45 min at 4 ºC to remove cell debris. The supernatant was loaded into a His-select Nickel Affinity Gel (Sigma) column pre-equilibrated with buffer A. Beads were first washed with buffer A followed by buffer A with extra KCl (500 mM). Most of the fusion protein was eluted from the resin with buffer A containing 20 mM imidazole. The remaining His-tagged protein was eluted with buffer A containing 250 mM imidazole. The eluted protein was pooled and dialyzed against buffer B (50 mM HEPES pH 7.5, 150 mM NaCl, 5 mM $CaCl_2$,1 mM TCEP) and loaded into a S200 size-exclusion chromatography column (GE Healthcare), pre-equilibrated with buffer B.

Purification of large EAG1 channel fragments

Several constructs (cap-PAS-BDN, PAS-BDN and CNBhD-BDC1-BDC2) suffer proteolysis during expression in bacteria. To overcome this problem, these were cloned into MCS1 of vector pRSFDuet-1 with an N-terminal His_6-tag and CaM was cloned into MCS2 of the same vector without any affinity tag. Co-expression with CaM shields the mEAG1 the protein fragments from proteases. Expression and purification was performed as described in (Marques-Carvalho et al., 2012) except that the buffering agent was 50 mM HEPES pH 7.5. Despite the lack of calcium in the lysis and wash buffers, CaM still came attached to the eluted protein. To disrupt the complex, the eluted protein was dialyzed against buffer C (50 mM HEPES pH 7.5, 150 mM NaCl, 1 mM EDTA, 5 mM DTT). The dialyzed protein was loaded into a 5 mL Hitrap Q HP (GE Healthcare) equilibrated with buffer D (50 mM HEPES pH 7.5, 150 mM NaCl, 5 mM DTT). The mEAG1 fragment-enriched flow-through was collected, and CaM was eluted from the beads with a NaCl gradient. The channel fragment was further purified in a S200 size-exclusion chromatography column, pre-equilibrated with buffer B.

Expression and purification of CaM lobes and mutants

CaM lobes and the CaM-EF12 mutant (mutations D21A/D57A) were cloned as His_6-tagged MBP fusions and purified as described for the other MBP fusions. Briefly, cleared bacterial lysate was loaded into a His-select nickel affinity column and eluted with buffer A containing 20 and 250 mM imidazole. TEV protease was added to the eluted protein to cleave MBP-tag from the CaM lobes and dialyzed overnight against buffer B. After cleavage, the protein solution was further purified using nickel beads to bind the His_6-tagged TEV protease and MBP. Flow-through containing the lobe was kept. The solution was loaded into an affinity column MBPtrap (GE Healthcare) to remove any MBP contaminants. CaM lobes were further purified in a S200 size-exclusion chromatography column equilibrated in buffer B.

Purification of CaM-BDC2 for crystallization

Purification was as for BDC2 except that buffers included 5mM $CaCl_2$. After elution from Ni-beads, MBP tag was cleaved off overnight with TEV protease. A second step of Ni-beads bound most MBP and TEV protease. Flow-through containing the CaM-peptide complex was loaded into an affinity column MBPtrap to remove remaining MBP. Complex present in flow-through was further purified in a S200 size-exclusion chromatography column equilibrated with buffer E (20 mM HEPES pH 7.5,

INSTITUTO
DE INVESTIGAÇÃO
E INOVAÇÃO
EM SAÚDE
UNIVERSIDADE
DO PORTO

Rua Alfredo Allen, 208
4200-135 Porto
Portugal
+351 220 408 800
info@i3s.up.pt
www.i3s.up.pt

150 mM NaCl, 1 mM $CaCl_2$, 1 mM TCEP). Protein was concentrated to 780 µM (~16 mg/mL) before setting crystallization drops.

Expression and purification of PAS domain (mEAG1 1-137) for fluorescence spectroscopy.

Briefly, PAS domain was expressed at 37 ºC in *Escherichia coli* BL21 (DE3) in Luria broth medium supplemented with kanamycin (50 mg/L) until the 600 nm optical density reached 0.6–0.8. At this point, cultures were placed on ice for 30 min. Ethanol and IPTG were added to a final concentration of 2%(v/v) and 0.5 mM, respectively, for overnight induction at 18 ºC. The pelleted culture was resuspended in buffer F (50 mM Tris-HCl pH 8, 150 mM NaCl, 5 mM imidazole) supplemented with protease inhibitors. Cell lysis was performed in a cooled cell cracker (Emulsiflex-C5, Avestin) and the lysate was centrifuged at 32 800xg for 45 min at 4 ºC to remove cell debris. The supernatant was loaded into Ni-beads pre-equilibrated with buffer F and washed with buffer F until the 280 nm optical density stabilized. The beads were washed with buffer F + 300 mM NaCl and buffer F containing 20 mM imidazole. Protein was eluted with buffer F containing 150 mM imidazole. To remove imidazole, the eluted protein was dialyzed against buffer G (20 mM Tris-HCl pH 8.0, 150 mM NaCl and 5 mM DTT) and loaded into a S200 size-exclusion chromatography column (GE Healthcare), pre-equilibrated with the same buffer.

Labeling of PAS cysteines and Fluorescence assay to analyze the PAS-CNBh interaction

PAS was incubated with 1 mM TCEP for 1 h at 4 ºC to reduce cysteine residues. It was passed through a desalting column equilibrated with buffer H (20 mM Tris HCl pH 8.0, 150 mM NaCl) and incubated with fluorescein-5-maleimide (Molecular Probes) at molar ratios 1:5 and 1:10 for 1h at room temperature, protected from light. After 1 h the reaction was stopped with 5 mM DTT and dialyzed against buffer G using a 3.5 kDa cutoff dialysis membrane.

For the fluorescence assay fluorescently labeled PAS at 100 nM was incubated with different concentrations of CNB-homology domain in the dialysis buffer G for at least 20 min. Fluorescence anisotropy measurements were performed at 25 ºC in a Horiba Fluoromax-4 spectrofluorimeter using an excitation wavelength of 492 nm and emission of 514 nm, with slit widths of 1 or 2 nm. To estimate binding affinity, plots of the anisotropy versus total CNB-homology domain concentration were fit with:

$$\frac{\qquad}{\qquad}$$

in which Rt and Lt are total receptor and total ligand concentrations, respectively, K_D is the ligand-binding affinity, and α and β are a scaling factor and an offset factor, respectively.

Supplemental Reference:

INSTITUTO DE INVESTIGAÇÃO E INOVAÇÃO EM SAÚDE
UNIVERSIDADE DO PORTO

Rua Alfredo Allen, 208
4200-135 Porto
Portugal
+351 220 408 800
info@i3s.up.pt
www.i3s.up.pt

Marques-Carvalho, M.J., Sahoo, N., Muskett, F.W., Vieira-Pires, R.S., Gabant, G., Cadene, M., Schonherr, R., and Morais-Cabral, J.H. (2012). Structural, biochemical, and functional characterization of the cyclic nucleotide binding homology domain from the mouse EAG1 potassium channel. J Mol Biol *423*, 34-46.

INSTITUTO
DE INVESTIGAÇÃO
E INOVAÇÃO
EM SAÚDE
UNIVERSIDADE
DO PORTO

Rua Alfredo Allen, 208
4200-135 Porto
Portugal
+351 220 408 800
info@i3s.up.pt
www.i3s.up.pt